



1 Daytime formation of nitrous acid at a coastal remote site in 2 Cyprus indicating a common ground source of atmospheric 3 HONO and NO

4 Hannah Meusel, Uwe Kuhn¹, Andreas Reiffs², Chinmay Mallik², Hartwig Harder², Monica
5 Martinez², Jan Schuladen², Birger Bohn³, Uwe Parchatka², John N. Crowley², Horst Fischer²,
6 Thorsten Hoffmann⁴, Ruud Janssen^{2,5}, Oscar Hartogensis⁶, Michael Pikridas⁷, Mihalis
7 Vrekoussis^{7,8,9}, Efstratios Bourtsoukidis², Bettina Weber¹, Jos Lelieveld², Jonathan Williams²,
8 Ulrich Pöschl¹, Yafang Cheng¹, Hang Su¹

9 ¹Max Planck institute for Chemistry, Multiphase Chemistry Department, Mainz, Germany

10 ²Max Planck Institute for Chemistry, Atmospheric Chemistry Department, Mainz, Germany

11 ³Institute for Energy and Climate Research (IEK-8), Research Center Jülich, Jülich, Germany

12 ⁴Johannes Gutenberg University, Inorganic and Analytical Chemistry, Mainz, Germany

13 ⁵MeteoGroup, Wageningen, Netherlands

14 ⁶Wageningen University and Research Center, Meteorology and Air Quality, Wageningen, Netherlands

15 ⁷Cyprus Institute, Energy, Environment and Water Research Center, Nicosia, Cyprus

16 ⁸Institute of Environmental Physics and Remote Sensing – IUP, University of Bremen, Germany

17 ⁹Center of Marine Environmental Sciences – MARUM, University of Bremen, Germany

18 *Correspondence to:* Hang Su (h.su@mpic.de)

19 **Abstract.** Characterization of daytime sources of nitrous acid (HONO) is crucial to understand atmospheric
20 oxidation and radical cycling in the planetary boundary layer. HONO and numerous other atmospheric trace
21 constituents were measured on the Mediterranean island of Cyprus during the CYPHEX campaign (CYPHEX =
22 CYprus PHotochemical EXperiment) in summer 2014. Average volume mixing ratios of HONO were 35 pptv (\pm 25
23 pptv) with a HONO/NO_x ratio of 0.33, which was considerably higher than reported for most other rural and urban
24 regions. Diel profiles of HONO showed peak values in the late morning (60 \pm 28 pptv around 09:00 local time), and
25 persistently high mixing ratios during daytime (45 \pm 18 pptv) indicating that the photolytic loss of HONO is
26 compensated by a strong daytime source. Budget analyses revealed unidentified sources producing up to 3.4 x 10⁶
27 molecules cm⁻³ s⁻¹ of HONO and up to 2.0 x 10⁷ molecules cm⁻³ s⁻¹ NO. Under humid conditions (RH >70%), the
28 source strengths of HONO and NO exhibited a close linear correlation (R²=0.78), suggesting a common source that
29 may be attributable to emissions from microbial communities on soil surfaces.

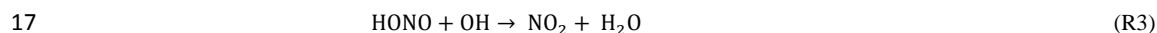
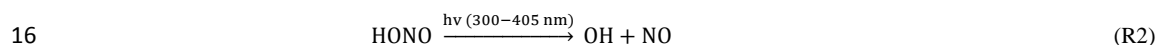
30 1 Introduction

31 Nitrous acid (HONO) is an important component of the nitrogen cycle being widely spread in the environment.
32 Either in its protonated form (HONO or HNO₂) or as nitrite ions (NO₂⁻) it can be found in the gas phase, on aerosol-
33 particles, in clouds and dew droplets but also in soil, sea-water and sediments (Foster et al., 1990; Rubio et al., 2002;
34 Acker et al., 2005 and 2008; Bianchi et al., 1997). It plays a key role in the oxidizing capacity of the atmosphere, as
35 it is an important precursor of the OH radical, which initiates most atmospheric oxidations. OH radicals react with
36 pollutants in the atmosphere to form mostly less toxic compounds (e.g. CO + OH → CO₂ + H₂O; Levy, 1971).



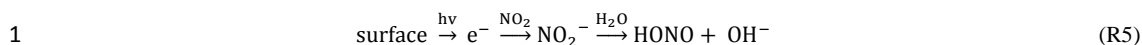
1 Volatile organic compounds (VOCs) react with OH contributing to formation of secondary aerosols (SOA), which
 2 can serve as cloud condensation nuclei CCN (Arey et al., 1990; Duplissy et al., 2008). Furthermore OH oxidizes SO₂
 3 to H₂SO₄, which condense subsequently to form aerosol particles (Zhou et al. 2013). In this way HONO has an
 4 indirect effect on the radiative budget and climate. In the first 2-3 hours following sunrise, when OH production from
 5 other sources (photolysis of O₃ and formaldehyde) is relatively low, photolysis of HONO can be the major source of
 6 OH radicals as HONO concentrations may be high after accumulation during night time (Lammel and Cape, 1996;
 7 Czader et al., 2012; Mao et al., 2010). On average up to 30% of the daily OH budget in the boundary layer is
 8 provided by HONO photolysis (Alicke et al., 2002; Kleffmann et al., 2005; Ren et al., 2006), but has been reported
 9 as high as 56% (Ren et al., 2003) with ambient HONO mixing ratios ranging from several pptv in rural areas up to a
 10 few ppb in highly polluted regions (Acker et al., 2006a and 2006b; Costabile et al., 2010; Li et al., 2012; Michoud et
 11 al., 2014; Spataro et al., 2013; Su et al. 2008a; Zhou et al., 2002a).

12 In early studies, atmospheric HONO was assumed to be in a photostationary state during daytime controlled by the
 13 gas phase reaction of NO and OH (R1) and two loss reactions which are the photolysis (R2) and the reaction with
 14 OH (R3).



18 However, field measurements in remote and rural locations, as well as urban and polluted regions found several
 19 times higher daytime HONO concentrations than model predictions, suggesting a large unknown source (Kleffmann
 20 et al., 2003 and 2005; Su et al., 2008a; Soergel et al., 2011a; Su et al., 2011; Michoud et al., 2014; Czader et al.,
 21 2012; Wong et al., 2013; Tang et al., 2015; Oswald et al., 2015) even after considering direct emission of HONO
 22 from combustion sources (Kessler and Platt, 1984; Kurtenbach et al., 2001). Heterogeneous reactions on aerosols
 23 have been proposed as an explanation for the missing source. The hydrolysis (R4, Finlayson-Pitts et al., 2003) and
 24 redox reactions of NO₂ have been intensively investigated on different kinds of surface such as fresh soot, aged or
 25 organic-coated particles (Amman et al., 1998; Arens et al., 2001; Aubin et al., 2007; Bröske et al., 2003; Han et al.,
 26 2013; Kalberer et al., 1999; Kleffmann et al., 1999; Kleffmann and Wiesen, 2005; Lelievre et al., 2004). Minerals
 27 like SiO₂, CaCO₃, CaO, Al₂O₃, and Fe₂O₃ showed a catalytic effect on the hydrolysis of NO₂ (Kinugawa et al., 2011;
 28 Liu et al., 2015; Wang et al., 2003; Yabushita et al., 2009). Different kind of surfaces (humic acid and other organic
 29 compounds, titanium dioxide, soot) can be photochemically activated which leads to enhanced NO₂ uptake and
 30 HONO production (R5, George et al., 2005; Langridge et al., 2009; Monge et al., 2010; Ndour et al., 2008; Ramazan
 31 et al., 2004; Stemmler et al., 2007; Kebede et al., 2013). The photolysis of particulate nitric acid (HNO₃), nitrate
 32 (NO₃⁻) and nitro-phenols (R-NO₂) lead to HONO formation as well (Baergen and Donaldson, 2013; Bejan et al.,
 33 2006; Ramazan et al., 2004; Scharko et al., 2014; Zhou et al., 2003; Zhou et al., 2011). But these reactions cannot
 34 account for the HONO levels observed during daytime (Elshorbany et al., 2012).





2 On the other hand, soil nitrite, either biogenic or non-biogenic, has been suggested as an effective source of HONO
3 (Su et al., 2011; Oswald et al., 2013). Depending on soil properties such as pH and water content and according to
4 Henry's law HONO can be released (Donaldson et al., 2014b; Su et al., 2011). This is consistent with field flux
5 measurements showing HONO emission from the ground rather than deposition as is the case for HNO₃ (Harrison
6 and Kitto, 1994; Kleffmann et al., 2003; Ren et al., 2011; Stutz et al., 2002; VandenBoer et al., 2013; Villena et al.,
7 2011; Wong et al., 2012 and 2013; Zhou et al., 2011). In a recent study, Weber et al. (2015) measured large HONO-
8 and NO-emissions from dryland soils with microbial surface communities (so-called biological soil crusts).
9 Several field studies also show a correlation of the unknown HONO source with solar radiation or the photolysis
10 frequency of NO₂ J_{NO2} (Su et al., 2008a; Sörgel et al., 2011a; Wong et al., 2012; Costabile et al., 2010; Michoud et
11 al., 2014, Oswald et al., 2015). This correlation can be explained either by the aforementioned photosensitized
12 reactions or by temperature-dependent soil-atmosphere exchange (Su et al., 2011). According to Su et al. (2011), the
13 release of HONO from soil surfaces is controlled by both the soil (biogenic and chemical) production of nitrite and
14 the gas-liquid phase equilibrium. The solubility is strongly temperature-dependent, resulting in a higher HONO
15 emission during noon time and high radiation J_{NO2} periods, and lower HONO emissions or even HONO deposition
16 during the nighttime as further confirmed by VandenBoer et al. (2015). This temperature dependence not only exists
17 for equilibrium over soil solution but also exists for adsorption/desorption equilibrium over dry and humid soil
18 surfaces (Li et al., 2016).
19 In this study we measured HONO and a suite of other atmospherically relevant trace gases in a coastal area on the
20 Mediterranean Island Cyprus in summer 2014. Due to low local anthropogenic impact and low NO_x levels in aged
21 air masses, but high solar radiation, this is an ideal site to investigate possible HONO sources and to gain a better
22 understanding of HONO chemistry.

23 **2 Instrumentation**

24 HONO was measured with a commercial Long Path Absorption Photometry instrument (effective light path 1.5 m,
25 LOPAP, Quma, Wuppertal, Germany). LOPAP has a collecting efficiency of >99% for HONO and a detection limit
26 of 4 pptv at a time resolution of 30s. To avoid potential interferences induced by long inlet lines and heterogeneous
27 formation or loss of HONO on the inlet walls, respectively (Kleffmann et al., 1998; Zhou et al., 2002b; Su et al.,
28 2008b), HONO was collected by a sampling unit installed directly in the outdoor atmosphere, i.e., placed on a mast
29 at a height of 5.8 meters above ground installed at the edge of a laboratory container. Furthermore, the LOPAP has
30 two stripping coils placed in series to reduce known interfering signals (Heland et al., 2001). In the first stripping coil
31 HONO is quantitatively collected. Due to the acidic stripping solution interfering species are collected less
32 efficiently but in both channels. The true concentration of HONO is obtained by subtracting the inferences quantified
33 in the second channel (in this study average 1 pptv, at most 5 pptv) from the total signal obtained from the first
34 channel. For a more detailed description of LOPAP, see Heland et al. (2001). This correction of chemical
35 interferences ascertained excellent agreement with the (absolute) DOAS measurements, both in a smog chamber and
36 under urban atmospheric conditions (Kleffmann et al., 2006). A possible interference from peroxyntic acid (HNO₄)



1 has been proposed (Liao et al., 2006; Kerbrat et al., 2012; Legrand et al., 2014), but this will be insignificant at the
2 high temperatures during CYPHEX, at which HNO_4 is unstable. The stripping coils are temperature controlled by a
3 water-based thermostat and the whole external sampling unit is shielded from sunlight by a small plastic housing.
4 The reagents were all high purity grade chemicals, i.e., hydrochloric acid (37%, for analysis; Merck), sulfanilamide
5 (for analysis, >99%; AppliChem) and N-(1-naphthyl)-ethylenediamine dihydrochloride (for analysis, >98%;
6 AppliChem). For calibration Titrisol® 1000 mg NO_2^- (NaNO_2 in H_2O ; Merck) was diluted to 0.0015 and 0.005 mg/L
7 NO_2^- . For preparation all solutions and for cleaning of the absorption tubes 18 M Ω H_2O was used.
8 NO and NO_2 measurements were made with a modified commercial chemiluminescence Detector (CLD 790 SR)
9 originally manufactured by ECO Physics (Duernten, Switzerland). The two-channel CLD based on the
10 chemiluminescence of the reaction between NO and O_3 was used for measurements of NO and NO_2 . NO_2 was
11 measured as NO using a photolytic converter from Droplet Measurement Technologies, Boulder USA. In current
12 study, data were obtained at a time resolution of 5 seconds. The CLD detection limits (determined by continuously
13 measuring zero air at measuring site) for NO and NO_2 measurements were 5 pptv and 20 pptv, respectively for an
14 integration period of 5 s. O_3 was measured with a standard UV photometric detector (Model 49, Thermo
15 Environmental Instruments Inc.) with a detection limit of 1 ppb. Data are reported for an integration period of 60 s.
16 The total uncertainties (2σ) for the measurements of NO, NO_2 and O_3 were determined to be 20%, 30% and 5%,
17 respectively, based on the reproducibility of in-field background measurements, calibrations, the uncertainties of the
18 standards and the conversion efficiency of the photolytic converter (Li et al., 2015).
19 OH and HO_2 radicals were measured using the HydrOxyl Radical measurement Unit based on fluorescence
20 Spectroscopy (HORUS) setup developed at the Max Planck Institute for Chemistry (Mainz, Germany). HORUS is
21 based on laser induced fluorescence- fluorescence assay by gas expansion (LIF-FAGE) technique, wherein OH
22 radicals are selectively excited at low pressure by pulsed UV light at around 308 nm, and the resulting fluorescence
23 of OH is detected using gated microchannel plate (MCP) detectors (Martinez et al., 2010; Hens et al., 2014). HO_2 is
24 estimated by converting atmospheric HO_2 into OH using NO, and detecting the additional OH formed. The
25 instrument is calibrated by measuring signals from known amounts of OH and HO_2 generated by photolysis of water
26 vapor in humidified zero air.
27 Photolysis frequencies were determined using a spectroradiometer (Metcon GmbH) with a single monochromator
28 and 512 pixel CCD-array as detector (275-640 nm). The thermostatted monochromator/detector unit was attached via
29 a 10 m optical fiber to a 2- Π integrating hemispheric quartz dome. The spectroradiometer was calibrated prior to the
30 campaign using a 1000 W NIST traceable irradiance standard. J-values were calculated using molecular parameters
31 recommended by the IUPAC and NASA evaluation panels (Sander et al., 2011; IUPAC, 2015). The J-value for
32 HONO was not corrected for upwelling UV radiation and is estimated to have an uncertainty of ~10 % (Bohn et al.,
33 2008).
34 Aerosol measurements were also performed during the campaign. In this study particulate nitrate and aerosol surface
35 data were used. These were detected by high resolution – time of flight – aerosol mass spectrometer (HR-ToF-AMS,
36 Aerodyne Research Inc., Billerica, MA USA) and scanning mobility particle sizer (SMPS 3936, TSI, Shoreview,
37 MN USA) and aerodynamic particle sizer (APS 3321, TSI), respectively. The mobility and aerodynamic based size
38 distributions were combined based on the algorithm proposed by Khlystov et al. (2004).



1 The volatile organic compounds (VOC) including α -pinene, β -pinene, isoprene, Δ^3 -carene, limonene and DMS
2 (dimethyl sulfide) were detected by a commercial Gas Chromatography-Mass Spectrometry (GC-MS) system (MSD
3 5973; Agilent Technologies GmbH) coupled with an air sampler and a thermal desorber unit (Markes International
4 GmbH). The VOCs were trapped at 30°C on a low-dead-volume quartz cold trap (U-T15ATA; Markes International
5 GmbH) filled with two bed sorbent (Tenax TA and Carbograph I). The cold trap was heated to 320°C and the sample
6 was transferred to a 30m GC column (DB-624, 0.25mm I.D., 1.4 μ m film; J&W Scientific). The temperature of the
7 GC oven was programmed to be stable at 40°C for 5mins and then rising with a rate of 5°C/min up to 140°C.
8 Following, the rate was increased to 40°C/min up to 230°C where it was stabilized for 3min. Each sample was taken
9 every 45mins and calibrations, using a commercial gas standard mixture (National Physical Laboratory, UK), were
10 performed every 8-12 samples.

11 Formaldehyde (HCHO) was measured with a commercial analyzer based on the Hantzsch reaction. The product of
12 the reaction of HCHO with acetyl-acetone and ammonia absorbs light at 410 nm and fluoresces at 510 nm which is
13 detected (AL4011, Aerolaser GmbH, Garmisch-Partenkirchen, Germany).

14 Carbon monoxide was measured by infrared absorption spectroscopy using a room temperature quantum cascade
15 laser at a time resolution of 1 s. Data are reported as 60 s averages with a total uncertainty of ~10% mainly
16 determined by the uncertainty of the used NIST standard (Li et al., 2015).

17 Meteorological parameters (temperature, relative humidity, wind speed and wind direction, pressure, solar radiation,
18 precipitation) were detected by the weather station Vantage Pro2 from DAVIS.

19 Besides GC-MS all other operating instruments had time resolutions between 20 s and 5 min. For most analyses in
20 this study the data were averaged to 10 min. When GC-MS data were included in the evaluation 1 hour averaged data
21 were used.

22 3 Site description

23 Cyprus is a 9251 km² island in the South-East Mediterranean Sea (fig. 1). The measuring site was located on a
24 military compound in Ineia, Cyprus (N 34.9638, E 32.3778), about 600 m above sea level and approximately 5.5 - 8
25 km from the coast line (in the main wind direction W-SW). The field site is characterized by light vegetation cover,
26 mainly comprising small shrubs like *Pistacia lentiscus*, *Sacopoterium spinosum*, and *Nerium oleander*, herbs like
27 *Inula viscosa* and *Foeniculum vulgare* and few typical Mediterranean trees like *Olea europaea*, *Pinus* sp., and
28 *Ceratonia siliqua*. The area within a radius of about 15 km around the station is only weakly populated. Paphos
29 (88,266 citizens) is located 20 km south of the field site, Limassol (235,000), Nicosia (325,756) and Larnaca
30 (143,367) are 70, 90 and 110 km in the E-SE, respectively (population data according to statistical service of the
31 republic of Cyprus, www.cystat.gov.cy, census of population Oct 2011). During the campaign (07.07. - 04.08.2014),
32 clear sky conditions prevailed and occasionally clouds skimmed the site. No rain was observed, but the elevated field
33 site was impacted by fog during nighttime and early morning due to adiabatic cooling of ascending marine humid air
34 masses. Temperature ranged from 18 to 28°C. Within the main local wind direction of SW (fig. 2A) there was no
35 direct anthropogenic influence resulting in clean humid air from the sea. Analysis of 48-hours back trajectories
36 showed mainly two source regions of air mass origin (fig. 2B). Approximately half (46%) of the campaign the air



1 masses came from the West of Cyprus spending most of their time over the Mediterranean Sea prior to arriving at the
2 site. During the remaining half of the campaign air masses originated from the North of Cyprus, from East European
3 countries (Turkey, Bulgaria, Rumania, Ukraine and Russia). Westerly air masses have been shown to exhibit lower
4 concentration of gaseous and aerosol pollutants than the predominant northerly air masses that typically reach the
5 site (Kleanthous et al., 2014). They spent more time over continental terrestrial surface and were likely to be
6 additionally affected by biomass burning events detected in East Europe within the measurement periods (FIRMS,
7 MODIS, web fire mapper, fig. S1). Previous back trajectory studies in the eastern Mediterranean support this
8 assumption (Kleanthous et al., 2014; Pikridas et al., 2010).
9 Most of the time the advected air mass was loaded with high humidity as a result of sea breeze circulation. Two
10 periods of about 4 days with lower relative humidity occurred. These two situations will be contrasted below.

11 **4 Results**

12 The concentrations of HONO and other atmospheric trace gases as well as meteorological conditions observed on
13 Cyprus from 7th July 2014 to 3rd August 2014 are shown in fig. 3. In general, low trace gas mixing ratios were
14 indicative of clean marine atmospheric boundary conditions, as pollutants are oxidized by OH during the relatively
15 long air transport time over the Mediterranean sea (more than 30 h), and without significant impact of direct
16 anthropogenic emissions.

17 Ambient HONO mixing ratios ranged from below detection limit (< 4 pptv) to above 300 pptv. Daily average HONO
18 was 35 pptv (± 25 pptv). The daily average NO_2 and NO mixing ratios were 140 ± 115 and 20 ± 35 pptv
19 respectively, but showed intermittent peaks up to 50 ppbv when sampling air was streamed from the diesel generator
20 used to power the station, from the access route or the parking lot by local winds (easterly, fig S2). These incidents,
21 which account for 4% of the campaign time, were classified as local air pollution events and were omitted from
22 analysis. Mean O_3 and CO mixing ratios were 72 ± 12 ppb and 98 ± 11 ppbv respectively. OH radicals ranged from
23 below detection limit (1×10^5 molecules cm^{-3}) during nighttime to 8×10^6 molecules cm^{-3} during daytime. Daytime
24 HO_2/OH ratio ranged from 100 to 150. The mixing ratios of NO_2 , O_3 and CO varied in unison, and were significantly
25 ($p < 0.05$) higher during periods when air masses originated from East Europe (brownish bar in fig. 3a lower panel),
26 indicative of air pollution and shorter transport times compared to western Europe (NO_2 : Northerly: 144 ± 130 pptv,
27 westerly: 127 ± 106 pptv; O_3 : Northerly: 74 ± 11 ppbv, westerly: 66 ± 12 ppbv; CO: Northerly: 101 ± 9 ppbv,
28 westerly: 90 ± 10 ppbv). In contrast, NO and HONO mixing ratios were slightly higher when air masses came from
29 Western Europe and over the sea (NO: Northerly: 17 ± 35 pptv, westerly: 20 ± 44 pptv; HONO: Northerly: 32 ± 26
30 pptv, westerly: 38 ± 22 pptv).

31 Besides two different air mass origins, two periods with different behaviour of relative humidity were identified
32 illustrated by blue and yellow boxes in fig. 3(a and b). In both periods we found northerly and westerly air mass
33 origins. The diel profiles of trace gas mixing ratios and meteorological variables of the humid period (blue box) are
34 shown in Fig. 4a, the ones of the dry period (yellow box) in Fig 4b. During the drier period HONO concentrations
35 are stable and low (6 pptv) during night, while mean nighttime HONO mixing ratios during the humid period (fig.
36 4a) showed an expected slow increase of about 20 pptv (from 20 to 40 pptv), as anticipated from heterogeneous



1 production and accumulation within a nocturnal boundary layer characterized by a stable stratification and low wind
2 speed (Acker et al., 2005; Su et al., 2008b; Li et al., 2012). During both periods, but more pronounced in the drier
3 period, HONO rapidly increased by a factor of 2 within two hours after sunrise and then slowly decreased until
4 sunset. Similar profiles were also observed for other trace gases like isoprene or DMS which are transported in
5 upslope winds. Strong HONO morning peaks and high daytime mixing ratios suggest a strong daytime source,
6 compensating the short atmospheric lifetime (15 min) caused by fast photolysis.

7 Mean NO mixing ratios were close to the detection limit (2 pptv) during night and increased after sunrise (06:00
8 local time LT) to mean values of 60 pptv (peak 150 pptv) at 09:00 LT, prior to declining for the rest of the day until
9 sunset (20:00 LT). In the absence of local NO sources low nighttime values are a result of the conversion of NO to
10 NO₂ by O₃ (Hosaynali Beygi et al., 2011). The diel profiles of NO mixing ratios followed closely those of HONO
11 mixing ratios. This similarity and their dependency on relative humidity are suggestive of a common source for both
12 reactive nitrogen species.

13 NO₂ mixing ratios were somewhat lower during nighttime, but in general the diel variability remained in a narrow
14 range between 100 and 200 pptv. Likewise, the diel courses of O₃ and CO mixing ratios revealed relatively low
15 day/night variability in a range of 65-75 and 90-100 ppb, respectively.

16 5 Discussion

17 Low NO_x conditions at this remote field site in photochemically aged marine air were found to be an ideal
18 prerequisite to trace yet un-defined local HONO sources. On Cyprus, diel profiles of HONO showed peak values in
19 the late morning and persistently high mixing ratios during daytime, as has been reported for some other remote
20 regions (Acker et al., 2006a; Zhou et al., 2007; Huang et al., 2002). This is not the case for rural and urban sites,
21 where atmospheric HONO mixing ratios are normally observed to continuously build up during nighttime
22 presumably due to heterogeneous reactions involving NO_x and decline in the morning due to strong
23 photodissociation (e.g., Elshorbany et al., 2012 and references therein).

24 The diel HONO/NO_x ratio (fig. 4a+b, third panel) shows consistently high values during the humid period (fig. 4a)
25 and significant diel variation for the dry case (fig. 4b) with higher values during day. The ratio (average 0.33 and
26 peak values greater than 2) is higher than that reported for most other regions, suggesting a strong impact of local
27 HONO sources. Elshorbany et al. (2012) investigated data from 15 different urban and rural field measurement
28 campaigns around the globe, and came up with a robust representative mean atmospheric HONO/NO_x ratio as low
29 as 0.02. However, high values were observed at remote mountain sites, with mean values of 0.23 (up to ≈0.5 in the
30 late morning; Zhou et al., 2007) or 0.2–0.4 at remote arctic/polar sites (Li, 1994; Zhou et al., 2001; Beine et al.,
31 2001; Jacobi et al., 2004; Amoroso et al., 2010). Legrand et al. (2014) observed HONO/NO_x ratios between 0.27 and
32 0.93 during experiments with irradiated Antarctic snow depending on radiation wavelength, temperature and nitrate
33 content. Elevated HONO/NO_x ratios at low NO_x levels show the importance of HONO formation mechanisms other
34 than heterogeneous NO_x reactions.



1 5.1 Nighttime HONO accumulation

2 Between 18:30 – 7:30 LT HONO has an atmospheric lifetime of more than 45 min and [OH] is low, just about 1×10^5
3 molecules cm^{-3} , so that the calculation of HONO at photostationary state $[\text{HONO}]_{\text{pss}}$ (R1-R3) at night is not
4 appropriate. Instead, nighttime HONO concentrations can be estimated due to heterogeneous reaction of NO_2
5 described in Eq. (1). Three studies in different environments from a rural forest region in East Germany (Sörgel et
6 al., 2011b) and a non-urban site in the Pearl River delta, China (Su et al., 2008b) to a urban, polluted site in Beijing
7 (Spataro et al., 2013) found a conversion rate of $1.6\% \text{ h}^{-1}$.

$$8 \quad [\text{HONO}]_{\text{het}} = [\text{HONO}]_{\text{evening}} + 0.016 \text{ h}^{-1} [\text{NO}_2] \Delta t, \quad (\text{Eq. 1})$$

9 $[\text{HONO}]_{\text{het}}$ denotes the accumulation of HONO by heterogeneous conversion of NO_2 , $[\text{HONO}]_{\text{evening}}$ the measured
10 HONO mixing ratio at 18:30 LT, $[\text{NO}_2]$ the measured average NO_2 mixing ratio between 18:30 and 7:30 LT, Δt time
11 span in hours.

12 Measured and calculated HONO mixing ratios are compared in figure 4 (upper panel). During the humid period,
13 during night the estimated (according Eq. (1), fig. 4a upper panel, grey line) and observed HONO mixing ratios are
14 in good agreement ($R^2 = 0.9$). During the drier period the observed HONO mixing ratios were lower than the ones
15 calculated with a NO_2 conversion rate of $1.6\% \text{ h}^{-1}$. But Kleffmann et al., 2003 found a smaller conversion rate of $6 \times$
16 10^{-7} s^{-1} ($0.22\% \text{ h}^{-1}$) for rural forested land in Germany which matches better to the observed nighttime HONO
17 concentration during drier period (fig. 4b upper panel, dark grey line).

18 As already mentioned above, it is apparent that under low RH conditions during night, HONO mixing ratios were
19 much lower than under humid conditions, and HONO morning peaks were most pronounced (compare Fig. 4a and
20 4b: humid/dry). Both HONO (Donaldson et al., 2014a) and NO_2 (Wang et al., 2012; Liu et al., 2015) uptake
21 coefficients have recently been reported to be much stronger for dry soil, or at low RH, respectively, which is in line
22 with HONO on Cyprus being close to the detection limit in nights with low relative humidity. On the other hand, it
23 has been shown on glass and on soil proxies that the yield of HONO formation from NO_2 on surfaces is low under
24 dry conditions, but sharply increases at $\text{RH} > 30\%$ (Liu et al., 2015) or $> 60\%$ (Finlayson-Pitts et al., 2003). On
25 Cyprus the strong morning HONO peaks after dry nights were accompanied by an increase in relative humidity from
26 40 to 80%. Deposited and accumulated NO_2 on dry soil surfaces could be released as HONO at high rates under
27 elevated RH conditions. In contrast, in a humid regime HONO mixing ratios were continuously high during
28 nighttime and showed less pronounced morning peaks, suggesting lower nighttime deposition of NO_2 and lower
29 HONO emissions in the morning, respectively.

30 As morning HONO peak mixing ratios were most pronounced after dry nights on Cyprus, our observations are to
31 some extent contradictory to earlier results that have proposed that dew formation on the ground surface may be
32 responsible for HONO nighttime accumulation in the aqueous phase, followed by release from this reservoir after
33 dew evaporation the next morning (Zhou et al., 2002a, Rubio et al., 2002, He et al., 2006). We cannot rule out that
34 the latter could have contributed to nighttime accumulation of HONO during humid conditions, as we had no means
35 to measure dew formation at the site, and high daytime HONO mixing ratios were observed under all humidity
36 regimes. However, kinetic models of competitive adsorption of trace gases and water onto particle surfaces predict
37 exchange behavior explicitly distinct from the liquid phase (Donaldson et al., 2014a). The nitrogen composition in



1 thin water films (few water molecular monolayers) is complex, including HONO, NO, HNO₃, water–nitric acid
 2 complexes, NO₂⁺ and N₂O₄ (Finlayson-Pitts et al., 2003). With only small amounts of surface-bound water, nitric
 3 acid is largely undissociated HNO₃ and is assumed to be stabilized upon formation of the HNO₃–H₂O complexes
 4 (hydrates), which have unique reactivity compared to nitric acid water aqueous solutions, where it is dissociated H⁺
 5 and NO₃⁻ ions (Finlayson-Pitts et al., 2003). Likewise, HONO formation rates in surface bound water are about four
 6 orders of magnitude larger than expected for the aqueous phase reaction (Pitts et al., 1984).
 7 Diel HONO profiles very similar to those on Cyprus with a late morning maximum and late afternoon/early evening
 8 minimum have been observed at the Meteorological Observatory Hohenpeissenberg, a mountain-top site in Germany
 9 (Acker et al., 2006a) and by Zhou et al. (2007) at the summit of Whiteface Mountain in New York State. For the
 10 latter study, formation of dew could be ruled out as relative humidity was mostly well below saturation. Zhou et al.
 11 (2007) argued that the high HONO mixing ratios during morning and late morning can be explained by mountain up-
 12 slope flow of polluted air from the cities at the foot of the mountain that results from ground surface heating. On
 13 Cyprus the sea breeze, driven by the growing difference between sea and soil surface temperature, brings air to the
 14 site which interacted with the soil surface and vegetation and is loaded by respective trace gas emissions. This is
 15 endorsed by the simultaneous increase of DMS and isoprene, markers for transportation of marine air and emission
 16 by vegetation. In the late afternoon, when the surface cools, down-welling air from aloft would dominate, being less
 17 influenced by ground surface processes. Zhou et al. (2007) could show that noontime HONO mixing ratios and
 18 average NO_y during the previous 24-hour period were strongly correlated, much better than instantaneous
 19 HONO/NO_y or HONO/NO_x, which is in line with N-accumulation on soil surfaces as discussed above.

20 5.2 Daytime HONO budget

21 During daytime (7:30 to 18:00 LT, with HONO lifetime being less than 30 min), [HONO]_{PSS}, the photostationary
 22 HONO mixing ratios resulting from gas phase chemistry can be calculated according to Eq. (2) (Kleffmann et al.,
 23 2005):

$$24 \quad [\text{HONO}]_{\text{PSS}} = \frac{k_1[\text{OH}][\text{NO}]}{k_2[\text{OH}] + J_{\text{HONO}}} \quad (\text{Eq. 2})$$

25 where k_1 and k_2 are the rate constants for the gas phase HONO formation from NO and OH and the loss of HONO by
 26 reaction of HONO and OH, respectively (Atkinson et al., 2004). J_{HONO} is the photolysis frequency of HONO, which
 27 was measured with a spectroradiometer. [NO] is the observed NO mixing ratio. Since OH data were available only
 28 on a few days, diel variations of [OH] were averaged (see fig. S3).

29 As has been previously established by many other studies (Su et al., 2008b; Michoud et al., 2014; Soergel et al.,
 30 2011a), homogeneous gas-phase chemistry alone fails to reflect observed HONO mixing ratios. Observed daytime
 31 values were up to 30 times higher than calculated based on PSS, indicating strong additional local daytime sources of
 32 HONO. The strength of these sources (S_{HONO}) can be calculated by following equation:

$$33 \quad S_{\text{HONO}} = ([\text{HONO}]_{\text{measured}} - [\text{HONO}]_{\text{PSS}}) \cdot (k_2[\text{OH}] + J_{\text{HONO}}) \quad (\text{Eq. 3})$$

34 In the late morning (around 10:00 LT) the unknown source was at its maximum with peak production rates of up to
 35 3.4×10^6 molecules cm⁻³ s⁻¹, and a daytime average of about 1.3×10^6 cm⁻³ s⁻¹, which is in good agreement with other



1 studies at rural sites like a mountain site at Hohenpeissenberg $((3\pm 1) \times 10^6 \text{ cm}^{-3} \text{ s}^{-1})$, at $\text{NO}_x \approx 2 \text{ ppbv}$, Acker et al.,
 2 2006a), a deciduous forest site in Jülich $(3.45 \times 10^6 \text{ molecules cm}^{-3} \text{ s}^{-1})$, at $\text{NO} \approx 250 \text{ pptv}$, Kleffmann et al., 2005) and
 3 a pine forest site in South-West Spain $0.74 \times 10^6 \text{ molecules cm}^{-3} \text{ s}^{-1}$, at $\text{NO}_x \approx 1.5 \text{ ppbv}$, Sörgel et al., 2011a) but
 4 smaller than at urban sites in Houston $(4\text{-}6 \times 10^6 \text{ cm}^{-3} \text{ s}^{-1})$, at $\text{NO}_x \approx 6 \text{ ppbv}$, Wong et al., 2012), Beijing $(7 \times 10^6 \text{ cm}^{-3} \text{ s}^{-1})$,
 5 at $\text{NO}_x \approx 15 \text{ ppbv}$, Yang et al., 2014) and South China $(5.25 \pm 3.75 \times 10^6)$, at $\text{NO}_x \approx 20 \text{ ppbv}$, Li et al., 2012; or $1\text{-}4 \times 10^7$
 6 $\text{cm}^{-3} \text{ s}^{-1}$, at $\text{NO}_x \approx 35 \text{ ppbv}$, Su et al., 2008a).

7 The contributions of gas phase reactions and the heterogeneous reaction of NO_2 (conversion rate $1.6\% \text{ h}^{-1}$) to the
 8 HONO budget are illustrated in fig. 5, exemplary. For both periods the contributions are quiet similar just the
 9 absolute values are different. To compensate the strong loss via photolysis a comparable strong unknown source is
 10 necessary as the heterogeneous NO_2 conversion or the gasphase reaction of OH and NO are insignificant.

11 In polluted regions with moderate to high NO_x concentrations, HONO sources have often been linked with $[\text{NO}_2]$ or
 12 $[\text{NO}_x]$ (Acker et al., 2005, Li et al., 2012, Levy et al., 2014, Sörgel et al., 2011a, Wentzel et al., 2010). Under the
 13 prevailing low NO_x conditions during CYPHEX ($< 250 \text{ pptv}$), correlation analysis (see table 1) of S_{HONO} with NO_2
 14 ($R^2 = 0.44$) and $\text{NO}_2 \cdot \text{RH}$ ($R^2 = 0.46$) indicate no significant impact of instantaneous heterogeneous formation of
 15 HONO from NO_2 . Better correlations of S_{HONO} with J_{NO_2} ($R^2 = 0.74$) and $J_{\text{NO}_2} \cdot [\text{NO}_2]$ ($R^2 = 0.84$) indicate a photo-
 16 induced conversion of NO_2 to HONO as already suggested by George et al. (2005) or Stemmler et al. (2006, 2007).
 17 Other light dependent reactions such as the photolysis of nitrate might additionally contribute to high daytime
 18 HONO. It is unlikely that aerosol surfaces played an important role in heterogeneous conversion of NO_2 as the mean
 19 observed aerosol surface concentration was only about $300 \mu\text{m}^2 \text{ cm}^{-3}$. Based on a formula for photo enhanced
 20 conversion of NO_2 on humic acid aerosols which was derived by Stemmler et al. (2007) a HONO formation rate of
 21 only $5.1 \times 10^2 \text{ molecules cm}^{-3} \text{ s}^{-1}$ can be estimated. Likewise, Sörgel et al. (2015) showed that HONO fluxes from
 22 light-activated reactions of NO_2 on humic acid surfaces at low NO_2 levels ($< 1 \text{ ppb}$ and thus comparable to
 23 concentrations observed in this study) saturated at around $0.0125 \text{ nmol m}^{-2} \text{ s}^{-1}$. Therefore heterogeneous aerosol
 24 surface reactions can be neglected as HONO sources at the prevailing low NO_x levels.

25 Likewise, the nitrate concentrations of highly acidic marine aerosols particulate matter as measured by HR-ToF-
 26 AMS (PM1 fraction, mean $0.075 \mu\text{g m}^{-3}$) were too low to account for significant photolytic HONO production
 27 ($1.7 \times 10^2 \text{ molecules cm}^{-3} \text{ s}^{-1}$ or 0.01% of S_{HONO}) calculated by Eq. (4):

$$28 \quad S_{\text{photo_NO}_3^-} = [\overline{\text{NO}_3^-}] \cdot J_{\text{NO}_3^-} \quad (\text{Eq. 4})$$

29 with $S_{\text{photo_NO}_3^-}$ the source strength of HONO by photolysis of nitrate, $[\overline{\text{NO}_3^-}]$ the mean particulate nitrate
 30 concentration and $J_{\text{NO}_3^-}$ the photolysis frequency of nitrate (aq) at noon ($3 \times 10^{-7} \text{ s}^{-1}$, Jankowski et al., 1999).

31 Recently an enhancement of the photolysis frequency of particulate nitrate relative to gaseous or aqueous nitrate was
 32 found (Ye et al., 2016). But even with this enhanced rate of $2 \times 10^{-4} \text{ s}^{-1}$ not more than $1.1 \times 10^5 \text{ molecules cm}^{-3} \text{ s}^{-1}$ (8%
 33 of S_{HONO}) HONO would be produced.



1 5.3 Common daytime source of HONO and NO

2 During CYPHEX, good correlation was found between [HONO] or S_{HONO} and [NO] ($R^2 = 0.86$ and 0.64 ,
 3 respectively), indicating that both may have a common source. A missing source of NO based on the photostationary
 4 state can be calculated as shown in Eq. (5) and (6).

$$5 \quad [\text{NO}]_{\text{PSS}} = \frac{J_{\text{NO}_2}[\text{NO}_2] + J_{\text{HONO}}[\text{HONO}]}{k_1[\text{OH}] + k_3[\text{HO}_2] + k_4[\text{O}_3] + k_5[\text{RO}_2]} \quad (\text{Eq. 5})$$

$$6 \quad S_{\text{NO}} = ([\text{NO}]_{\text{measured}} - [\text{NO}]_{\text{PSS}}) \cdot (k_1[\text{OH}] + k_3[\text{HO}_2] + k_4[\text{O}_3] + k_5[\text{RO}_2]) \quad (\text{Eq. 6})$$

7 k_3 and k_4 are the rate constants for the reaction of NO with HO_2 and O_3 , respectively (Atkinson et al., 2004), k_5 is the
 8 rate constant for the reaction of NO and organic peroxy radicals which was assumed to be the same as for the
 9 reaction $\text{NO} + \text{CH}_3\text{O}_2$ ($7.7 \times 10^{-12} \text{ s}^{-1}$ at 298K, Ren et al., 2010; Sander et al., 2011). Like [OH] also [HO₂] was
 10 measured only on a few days and therefore mean diel data were used (fig. S3). Total [RO₂] was estimated to be
 11 maximum $1.6 \cdot [\text{HO}_2]$ (Ren et al., 2010; Hens et al., 2014). Using a RO_2/HO_2 ratio of 1.2 the absolute values of S_{NO}
 12 are reduced by 0.3 to 5.5%. The budget analysis for NO for both humidity regimes is illustrated in fig. S4.

13 For NO_x , an unexpected deviation from the PSS, or Leighton ratio, respectively, of clean marine boundary layer air
 14 has been observed previously, invoking a hitherto unknown NO sink, or pathway for NO to NO_2 oxidation, other
 15 than reactions with OH, HO_2 , O_3 and organic peroxides (Hosaynali Beygi et al., 2011). On Cyprus, two different
 16 atmospheric humidity regimes can be differentiated. Under dry conditions ($\text{RH} < 70\%$, yellow boxes in fig. 3) and
 17 higher NO_x concentrations ($>150 \text{ pptv}$) S_{NO} is negative, implying a net NO sink of up to $6.4 \times 10^7 \text{ molecules cm}^{-3} \text{ s}^{-1}$
 18 resembling the above mentioned PSS deviations in remote marine air masses (see fig. 6 and 7). However, during
 19 humid conditions ($\text{RH} > 70$, blue boxes in fig. 3) S_{NO} was positive with values of up to $5.1 \times 10^7 \text{ molecules cm}^{-3} \text{ s}^{-1}$.
 20 Due to low and invariant acetonitrile levels, anthropogenic activity and local biomass burning can be excluded as NO
 21 source at this specific site. A net NO source during humid conditions is assumed to result from (biogenic) NO
 22 emission from soil. As shown in fig. 8, the PSS-based S_{HONO} and S_{NO} (time of day-averaged, excluding 3 days as
 23 there are transition days 25.7. and 2.8. or the RH changed too quickly 15.7.) were highly correlated ($R^2 = 0.78$),
 24 indicative of both reactive N-compounds being emitted from the same local source. Both HONO and NO have been
 25 reported to be released from soil, with a strong dependency on soil water content (Su et al., 2011; Oswald et al.,
 26 2013). The (dry state) soil humidification threshold level for NO emission is reported to be somewhat higher than for
 27 HONO (Oswald et al., 2013), which might explain why a net PSS-based NO source was preferentially calculated for
 28 higher relative humidity conditions, while for HONO the PSS indicated a daytime source under all humidity regimes
 29 prevailing during the campaign. Analyzing microbial surface communities from drylands, Weber et al. (2015)
 30 observed highly correlated NO-N and HONO-N emissions with Spearman rank correlation coefficients ranging
 31 between 0.75 and 0.99. In this study, NO- and HONO-emissions were observed in drying soils with water contents
 32 of 20-30% water holding capacity.

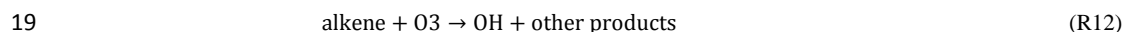
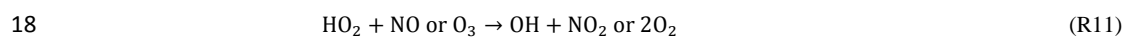
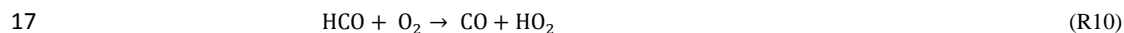
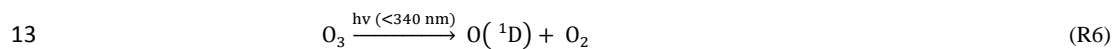
33 Even though we cannot make firm conclusions regarding the exact mechanism of HONO formation, the above
 34 mentioned correlation analysis (and table 1) reveal that the instantaneous heterogeneous NO_2 conversion is not a
 35 significant HONO source. We propose that HONO is emitted from nitrogen compounds being accumulated on
 36 mountain slope soil surfaces produced either biologically by soil microbiota or from previously deposited NO_y . This



1 forms the major daytime HONO source responsible for morning concentration peaks and consistently high daytime
 2 mixing ratios at the Cyprus field site. While biological formation is assumed to be more relevant for humid
 3 conditions, physical NO_y accumulation can be assumed to be stronger under dry conditions, as uptake coefficients
 4 for a variety of trace gases were shown to be significantly higher for dry surfaces, among them NO₂ (Wang et al.,
 5 2012, Liu et al., 2015), HONO (Donaldson et al. 2014a) and HCHO (Li et al., 2016). The strongest HONO morning
 6 peaks observed after dry nights were accompanied by an increase in relative humidity driven by the sea breeze (fig.
 7 4b), so we consider HONO being released preferentially under favourable humid conditions.

8 5.4 OH production

9 Many studies showed high contribution of HONO photolysis to the OH budget (up to 30% on daily average; Alicke
 10 et al., 2002, Ren et al., 2006). Here the OH production rates is calculated based on the main OH forming reactions,
 11 which are the photolysis of ozone and subsequent reaction with water (R6+7), the photolysis of HONO (R2) and
 12 HCHO (R8-11) and the reaction of alkenes with ozone (R12).



20 Reaction rates were taken from Atkinson et al. (2004) and Atkinson (1997). The water pressure over water was
 21 calculated according to Murphy and Koop (2005). Reactions of O(¹D) and HO₂ not forming OH are also considered.
 22 OH formation yields of the reactions of alkenes with O₃ were taken from Paulson et al. (1999). Photolysis rates (J-
 23 values) and concentrations of relevant compounds were as measured on Cyprus. Isoprene, α-pinene, β-pinene, Δ3-
 24 carene and limonene were taken into account as the most relevant alkenes.

25 The results of this study are shown in fig. 9. All four production routes show a clear diel profile with higher
 26 production rates during daytime. In the night only the reaction of alkene with O₃ produced significant amounts of OH
 27 (1.5 × 10⁴ molecules cm⁻³ s⁻¹). With sunrise the other sources become more relevant. The photolysis of HONO and
 28 HCHO lead to similar daytime OH production rates of about 0.8 – 1.7 × 10⁶ molecules cm⁻³ s⁻¹. The maximum OH
 29 production rate by O₃ photolysis during daytime is about 1.5 × 10⁷ molecules cm⁻³ s⁻¹. In the morning and evening
 30 hours the contribution of HONO photolysis to the total OH production is in average 30% (see fig. 9b) with peak
 31 values of 60%, which is much higher than the contribution of O₃ photolysis at that time. During the rest of the day
 32 the contribution decreases to 12%. The contribution of HCHO is slightly lower. At noon the most dominant OH
 33 source is the photolysis of O₃.



1 **6 Conclusion**

2 Nitrous acid was found in low concentrations on the east Mediterranean Island of Cyprus during summer 2014.
3 Daytime concentrations were much higher than during the night and about 30 times higher than would be expected
4 by budget analysis based on photostationary state. The unknown source was calculated to be about 1.9×10^6
5 molecules $\text{cm}^{-3} \text{ s}^{-1}$ around noon. Low NO_x concentrations, high HONO/ NO_x ratio and low correlation between
6 HONO and NO_2 indicate a local source which is independent from NO_2 . Heterogeneous reactions of NO_2 on aerosols
7 play an insignificant role during daytime. Emission from soil, either caused by photolysis of nitrate or gas-soil
8 partitioning of accumulated nitrite/nitrous acid, is supposed to have a higher impact on the HONO concentration
9 during this campaign. Also the NO budget analysis showed a missing source in the humid period, which correlates
10 well with the unknown source of HONO, indicating a common source. The most likely source of HONO and NO is
11 the emission from soil.
12 Even though the HONO concentration is only in the lower pptv level, it has a high contribution to the OH production
13 in the early morning and evening hours.

14 **Acknowledgement**

15 This study was supported by the Max Planck Society (MPG) and the DFG-Research Center / Cluster of Excellence
16 „The Ocean in the Earth System-MARUM”.
17 We thank the Cyprus Institute and the Department of Labor Inspection for the logistical support, as well as the
18 military staff at the Lara Naval Observatory in Ineia for the excellent collaboration.
19 Furthermore I'd like to thank Mathias Sörgel, an experienced colleague from MPI-C for his technical support on
20 experimental set-up of atmospheric HONO measurements.

21 **References**

22 Acker, K., Moller, D., Auel, R., Wieprecht, W., and Kalass, D.: Concentrations of nitrous acid, nitric acid, nitrite and
23 nitrate in the gas and aerosol phase at a site in the emission zone during ESCOMPTE 2001 experiment, Atmospheric
24 Research, 74, 507-524, 2005.
25 Acker, K., Moller, D., Wieprecht, W., Meixner, F. X., Bohn, B., Gilge, S., Plass-Dulmer, C., and Berresheim, H.:
26 Strong daytime production of OH from HNO₂ at a rural mountain site, Geophysical Research Letters, 33, 2006a.
27 Acker, K., Febo, A., Trick, S., Perrino, C., Bruno, P., Wiesen, P., Moeller, D., Wieprecht, W., Auel, R., Giusto, M.,
28 Geyer, A., Platt, U., and Allegrini, I.: Nitrous acid in the urban area of Rome, Atmospheric Environment, 40, 3123-
29 3133, 2006b.
30 Acker, K., Beysens, D., and Moeller, D.: Nitrite in dew, fog, cloud and rain water: An indicator for heterogeneous
31 processes on surfaces, Atmospheric Research, 87, 200-212, 2008.



- 1 Aliche, B., Platt, U., and Stutz, J.: Impact of nitrous acid photolysis on the total hydroxyl radical budget during the
2 Limitation of Oxidant Production/Pianura Padana Produzione di Ozono study in Milan, Journal of Geophysical
3 Research-Atmospheres, 107, 2002.
- 4 Ammann, M., Kalberer, M., Jost, D. T., Tobler, L., Rossler, E., Piguet, D., Gaggeler, H. W., and Baltensperger, U.:
5 Heterogeneous production of nitrous acid on soot in polluted air masses, Nature, 395, 157-160, 1998.
- 6 Amoroso, A., Domine, F., Esposito, G., Morin, S., Savarino, J., Nardino, M., Montagnoli, M., Bonneville, J. M.,
7 Clement, J. C., Ianniello, A., and Beine, H. J.: Microorganisms in Dry Polar Snow Are Involved in the Exchanges of
8 Reactive Nitrogen Species with the Atmosphere, Environmental Science & Technology, 44, 714-719, 2010.
- 9 Arens, F., Gutzwiller, L., Baltensperger, U., Gaggeler, H. W., and Ammann, M.: Heterogeneous reaction of NO₂ on
10 diesel soot particles, Environmental Science & Technology, 35, 2191-2199, 2001.
- 11 Arey, J., Atkinson, R., and Aschmann, S. M.: Product study of the gas-phase reactions of monoterpenes with the OH
12 radical in the presence of NO_x, Journal of Geophysical Research: Atmospheres, 95, 18539-18546, 1990.
- 13 Atkinson, R.: Gas-Phase Tropospheric Chemistry of Volatile Organic Compounds: 1. Alkanes and Alkenes, Journal
14 of Physical and Chemical Reference Data, 26, 215-290, 1997.
- 15 Atkinson, R., Baulch, D. L., Cox, R. A., Crowley, J. N., Hampson, R. F., Hynes, R. G., Jenkin, M. E., Rossi, M. J.,
16 and Troe, J.: Evaluated kinetic and photochemical data for atmospheric chemistry: Volume I - gas phase reactions of
17 O-x, HO_x, NO_x and SO_x species, Atmospheric Chemistry and Physics, 4, 1461-1738, 2004.
- 18 Aubin, D. G., and Abbatt, J. P. D.: Interaction of NO₂ with hydrocarbon soot: Focus on HONO yield, surface
19 modification, and mechanism, Journal of Physical Chemistry A, 111, 6263-6273, 2007.
- 20 Baergen, A. M., and Donaldson, D. J.: Photochemical Renoxification of Nitric Acid on Real Urban Grime,
21 Environmental Science & Technology, 47, 815-820, 2013.
- 22 Beine, H. J., Allegrini, I., Sparapani, R., Ianniello, A., and Valentini, F.: Three years of springtime trace gas and
23 particle measurements at Ny-Alesund, Svalbard, Atmospheric Environment, 35, 3645-3658, 2001.
- 24 Bejan, I., Abd El Aal, Y., Barnes, I., Benter, T., Bohn, B., Wiesen, P., and Kleffmann, J.: The photolysis of ortho-
25 nitrophenols: a new gas phase source of HONO, Physical Chemistry Chemical Physics, 8, 2028-2035, 2006.
- 26 Beygi, Z. H., Fischer, H., Harder, H. D., Martinez, M., Sander, R., Williams, J., Brookes, D. M., Monks, P. S., and
27 Lelieveld, J.: Oxidation photochemistry in the Southern Atlantic boundary layer: unexpected deviations of
28 photochemical steady state, Atmospheric Chemistry and Physics, 11, 8497-8513, 2011.
- 29 Bianchi, M., Feliatra, F., Tréguer, P., Vincendeau, M.-A., and Morvan, J.: Nitrification rates, ammonium and nitrate
30 distribution in upper layers of the water column and in sediments of the Indian sector of the Southern Ocean, Deep
31 Sea Research Part II: Topical Studies in Oceanography, 44, 1017-1032, 1997.
- 32 Bohn, B., Corlett, G. K., Gillmann, M., Sanghavi, S., Stange, G., Tensing, E., Vrekoussis, M., Bloss, W. J., Clapp, L.
33 J., Kortner, M., Dorn, H. P., Monks, P. S., Platt, U., Plass-Dulmer, C., Mihalopoulos, N., Heard, D. E., Clemitshaw,



- 1 K. C., Meixner, F. X., Prevot, A. S. H., and Schmitt, R.: Photolysis frequency measurement techniques: results of a
2 comparison within the ACCENT project, *Atmos. Chem. Phys.*, 8, 5373-5391, 2008.
- 3 Broske, R., Kleffmann, J., and Wiesen, P.: Heterogeneous conversion of NO₂ on secondary organic aerosol surfaces:
4 A possible source of nitrous acid (HONO) in the atmosphere?, *Atmospheric Chemistry and Physics*, 3, 469-474,
5 2003.
- 6 Costabile, F., Amoroso, A., and Wang, F.: Sub-mu m particle size distributions in a suburban Mediterranean area.
7 Aerosol populations and their possible relationship with HONO mixing ratios, *Atmospheric Environment*, 44, 5258-
8 5268, 2010.
- 9 Czader, B. H., Rappenglueck, B., Percell, P., Byun, D. W., Ngan, F., and Kim, S.: Modeling nitrous acid and its
10 impact on ozone and hydroxyl radical during the Texas Air Quality Study 2006, *Atmospheric Chemistry and*
11 *Physics*, 12, 6939-6951, 2012.
- 12 Donaldson, M. A., Berke, A. E., and Raff, J. D.: Uptake of Gas Phase Nitrous Acid onto Boundary Layer Soil
13 Surfaces, *Environmental Science & Technology*, 48, 375-383, 2014a.
- 14 Donaldson, M. A., Bish, D. L., and Raff, J. D.: Soil surface acidity plays a determining role in the atmospheric-
15 terrestrial exchange of nitrous acid, *Proceedings of the National Academy of Sciences*, 111, 18472-18477, 2014b.
- 16 Duplissy, J., Gysel, M., Alfarra, M. R., Dommen, J., Metzger, A., Prevot, A. S. H., Weingartner, E., Laaksonen, A.,
17 Raatikainen, T., Good, N., Turner, S. F., McFiggans, G., and Baltensperger, U.: Cloud forming potential of
18 secondary organic aerosol under near atmospheric conditions, *Geophysical Research Letters*, 35, 2008.
- 19 Elshorbany, Y. F., Steil, B., Brühl, C., and Lelieveld, J.: Impact of HONO on global atmospheric chemistry
20 calculated with an empirical parameterization in the EMAC model, *Atmos. Chem. Phys.*, 12, 9977-10000, 2012.
- 21 Finlayson-Pitts, B. J., Wingen, L. M., Sumner, A. L., Syomin, D., and Ramazan, K. A.: The heterogeneous
22 hydrolysis of NO₂ in laboratory systems and in outdoor and indoor atmospheres: An integrated mechanism, *Physical*
23 *Chemistry Chemical Physics*, 5, 223-242, 2003.
- 24 Foster, J. R., Pribush, R. A., and Carter, B. H.: THE CHEMISTRY OF DEWS AND FROSTS IN INDIANAPOLIS,
25 INDIANA, *Atmospheric Environment Part a-General Topics*, 24, 2229-2236, 1990.
- 26 George, C., Strekowski, R. S., Kleffmann, J., Stemmler, K., and Ammann, M.: Photoenhanced uptake of gaseous
27 NO₂ on solid-organic compounds: a photochemical source of HONO?, *Faraday Discussions*, 130, 195-210, 2005.
- 28 Han, C., Liu, Y., and He, H.: Role of Organic Carbon in Heterogeneous Reaction of NO₂ with Soot, *Environmental*
29 *science & technology*, 47, 3174-3181, 2013.
- 30 Harrison, R. M., and Kitto, A. M. N.: EVIDENCE FOR A SURFACE SOURCE OF ATMOSPHERIC NITROUS-
31 ACID, *Atmospheric Environment*, 28, 1089-1094, 1994.
- 32 He, Y., Zhou, X. L., Hou, J., Gao, H. L., and Bertman, S. B.: Importance of dew in controlling the air-surface
33 exchange of HONO in rural forested environments, *Geophysical Research Letters*, 33, 2006.



- 1 Heland, J., Kleffmann, J., Kurtenbach, R., and Wiesen, P.: A new instrument to measure gaseous nitrous acid
2 (HONO) in the atmosphere, *Environmental Science & Technology*, 35, 3207-3212, 2001.
- 3 Hens, K., Novelli, A., Martinez, M., Auld, J., Axinte, R., Bohn, B., Fischer, H., Keronen, P., Kubistin, D., Noelscher,
4 A. C., Oswald, R., Paasonen, P., Petaja, T., Regelin, E., Sander, R., Sinha, V., Sipila, M., Taraborrelli, D., Ernest, C.
5 T., Williams, J., Lelieveld, J., and Harder, H.: Observation and modelling of HO_x radicals in a boreal forest,
6 *Atmospheric Chemistry and Physics*, 14, 8723-8747, 2014.
- 7 Huang, G., Zhou, X. L., Deng, G. H., Qiao, H. C., and Civerolo, K.: Measurements of atmospheric nitrous acid and
8 nitric acid, *Atmospheric Environment*, 36, 2225-2235, 2002.
- 9 IUPAC: Task Group on Atmospheric Chemical Kinetic Data Evaluation, (Ammann, M., Cox, R.A., Crowley, J.N.,
10 Jenkin, M.E., Mellouki, A., Rossi, M. J., Troe, J. and Wallington, T. J.) <http://iupac.pole-ether.fr/index.html>, 2015.
- 11 Jacobi, H. W., Bales, R. C., Honrath, R. E., Peterson, M. C., Dibb, J. E., Swanson, A. L., and Albert, M. R.: Reactive
12 trace gases measured in the interstitial air of surface snow at Summit, Greenland, *Atmospheric Environment*, 38,
13 1687-1697, 2004.
- 14 Jankowski, J. J., Kieber, D. J., and Mopper, K.: Nitrate and nitrite ultraviolet actinometers, *Photochemistry and*
15 *Photobiology*, 70, 319-328, 1999.
- 16 Jiang, Q. Q., and Bakken, L. R.: Comparison of Nitrosospira strains isolated from terrestrial environments, *FEMS*
17 *Microbiology Ecology*, 30, 171-186, 1999.
- 18 Kalberer, M., Ammann, M., Arens, F., Gaggeler, H. W., and Baltensperger, U.: Heterogeneous formation of nitrous
19 acid (HONO) on soot aerosol particles, *Journal of Geophysical Research-Atmospheres*, 104, 13825-13832, 1999.
- 20 Kebede, M. A., Scharko, N. K., Appelt, L. E., and Raff, J. D.: Formation of Nitrous Acid during Ammonia
21 Photooxidation on TiO₂ under Atmospherically Relevant Conditions, *Journal of Physical Chemistry Letters*, 4,
22 2618-2623, 2013.
- 23 Kerbrat, M., Legrand, M., Preunkert, S., Gallée, H., and Kleffmann, J.: Nitrous acid at Concordia (inland site) and
24 Dumont d'Urville (coastal site), East Antarctica, *Journal of Geophysical Research: Atmospheres*, 117, D08303,
25 2012.
- 26 Kessler, C., and Platt, U.: Nitrous Acid in Polluted Air Masses — Sources and Formation Pathways, in: *Physico-*
27 *Chemical Behaviour of Atmospheric Pollutants*, edited by: Versino, B., and Angeletti, G., Springer Netherlands,
28 412-422, 1984.
- 29 Kinugawa, T., Enami, S., Yabushita, A., Kawasaki, M., Hoffmann, M. R., and Colussi, A. J.: Conversion of gaseous
30 nitrogen dioxide to nitrate and nitrite on aqueous surfactants, *Physical Chemistry Chemical Physics*, 13, 5144-5149,
31 2011.
- 32 Khlystov, A., Stanier, C., and Pandis, S. N.: An algorithm for combining electrical mobility and aerodynamic size
33 distributions data when measuring ambient aerosol, *Aerosol Science and Technology*, 38, 229-238, 2004.



- 1 Kleanthous, S., Vrekoussis, M., Mihalopoulos, N., Kalabokas, P., and Lelieveld, J.: On the temporal and spatial
2 variation of ozone in Cyprus, *Science of The Total Environment*, 476–477, 677–687, 2014.
- 3 Kleffmann, J., Becker, K. H., and Wiesen, P.: Heterogeneous NO₂ conversion processes on acid surfaces: possible
4 atmospheric implications, *Atmospheric Environment*, 32, 2721–2729, 1998.
- 5 Kleffmann, J., H. Becker, K., Lackhoff, M., and Wiesen, P.: Heterogeneous conversion of NO₂ on carbonaceous
6 surfaces, *Physical Chemistry Chemical Physics*, 1, 5443–5450, 1999.
- 7 Kleffmann, J., Kurtenbach, R., Lorzer, J., Wiesen, P., Kalthoff, N., Vogel, B., and Vogel, H.: Measured and
8 simulated vertical profiles of nitrous acid - Part I: Field measurements, *Atmospheric Environment*, 37, 2949–2955,
9 2003.
- 10 Kleffmann, J., Gavriolaiei, T., Hofzumahaus, A., Holland, F., Koppmann, R., Rupp, L., Schlosser, E., Siese, M., and
11 Wahner, A.: Daytime formation of nitrous acid: A major source of OH radicals in a forest, *Geophysical Research
12 Letters*, 32, 2005.
- 13 Kleffmann, J., and Wiesen, P.: Heterogeneous conversion of NO₂ and NO on HNO₃ treated soot surfaces:
14 atmospheric implications, *Atmospheric Chemistry and Physics*, 5, 77–83, 2005.
- 15 Kurtenbach, R., Becker, K. H., Gomes, J. A. G., Kleffmann, J., Lorzer, J. C., Spittler, M., Wiesen, P., Ackermann,
16 R., Geyer, A., and Platt, U.: Investigations of emissions and heterogeneous formation of HONO in a road traffic
17 tunnel, *Atmospheric Environment*, 35, 3385–3394, 2001.
- 18 Lammel, G., and Cape, J. N.: Nitrous acid and nitrite in the atmosphere, *Chemical Society Reviews*, 25, 361–369,
19 1996.
- 20 Langridge, J. M., Gustafsson, R. J., Griffiths, P. T., Cox, R. A., Lambert, R. M., and Jones, R. L.: Solar driven
21 nitrous acid formation on building material surfaces containing titanium dioxide: A concern for air quality in urban
22 areas?, *Atmospheric Environment*, 43, 5128–5131, 2009.
- 23 Legrand, M., Preunkert, S., Frey, M., Bartels-Rausch, T., Kukui, A., King, M. D., Savarino, J., Kerbrat, M., and
24 Jourdain, B.: Large mixing ratios of atmospheric nitrous acid (HONO) at Concordia (East Antarctic Plateau) in
25 summer: a strong source from surface snow?, *Atmos. Chem. Phys.*, 14, 9963–9976, 2014.
- 26 Lelièvre, S., Bedjanian, Y., Laverdet, G., and Le Bras, G.: Heterogeneous Reaction of NO₂ with Hydrocarbon Flame
27 Soot, *The Journal of Physical Chemistry A*, 108, 10807–10817, 2004.
- 28 Levy, H.: Normal Atmosphere: Large Radical and Formaldehyde Concentrations Predicted, *Science*, 173, 141–143,
29 1971.
- 30 Levy, M., Zhang, R., Zheng, J., Zhang, A. L., Xu, W., Gomez-Hernandez, M., Wang, Y., and Olaguer, E.:
31 Measurements of nitrous acid (HONO) using ion drift-chemical ionization mass spectrometry during the 2009
32 SHARP field campaign, *Atmospheric Environment*, 94, 231–240, 2014.
- 33 Li, J., A. Reiffs, U. Parchatka, and H. Fischer, In situ measurements of atmospheric CO and its correlation with NO_x
34 and O₃ at a rural mountain site, *Metrol.Meas. Syst.*, XXII, 25–38, 2015.



- 1 Li, S. M.: Equilibrium of particle nitrite with gas-phase HONO – tropospheric measurements in the high arctic
2 during sunrise, *Journal of Geophysical Research-Atmospheres*, 99, 25469-25478, 1994.
- 3 Li, X., Brauers, T., Haeseler, R., Bohn, B., Fuchs, H., Hofzumahaus, A., Holland, F., Lou, S., Lu, K. D., Rohrer, F.,
4 Hu, M., Zeng, L. M., Zhang, Y. H., Garland, R. M., Su, H., Nowak, A., Wiedensohler, A., Takegawa, N., Shao, M.,
5 and Wahner, A.: Exploring the atmospheric chemistry of nitrous acid (HONO) at a rural site in Southern China,
6 *Atmospheric Chemistry and Physics*, 12, 1497-1513, 2012.
- 7 Li, G., Su, H., Li, X., Kuhn, U., Meusel, H., Hoffmann, T., Ammann, M., Pöschl, U., Shao, M., and Cheng, Y.:
8 Uptake of gaseous formaldehyde by soil surfaces: a combination of adsorption/desorption equilibrium and chemical
9 reactions, *Atmos. Chem. Phys. Discuss.*, 2016, 1-29, 2016.
- 10 Liao, W., Case, A. T., Mastromarino, J., Tan, D., and Dibb, J. E.: Observations of HONO by laser-induced
11 fluorescence at the South Pole during ANTCI 2003, *Geophysical Research Letters*, 33, L09810, 2006.
- 12 Liu, Y., Han, C., Ma, J., Bao, X., and He, H.: Influence of relative humidity on heterogeneous kinetics of NO₂ on
13 kaolin and hematite, *Physical Chemistry Chemical Physics*, 17, 19424-19431, 2015.
- 14 Mao, J., Ren, X., Chen, S., Brune, W. H., Chen, Z., Martinez, M., Harder, H., Lefer, B., Rappenglück, B., Flynn, J.,
15 and Leuchner, M.: Atmospheric oxidation capacity in the summer of Houston 2006: Comparison with summer
16 measurements in other metropolitan studies, *Atmospheric Environment*, 44, 4107-4115, 2010.
- 17 Martinez, M., Harder, H., Kubistin, D., Rudolf, M., Bozem, H., Eerdeken, G., Fischer, H., Kluepfel, T., Gurk, C.,
18 Koenigstedt, R., Parchatka, U., Schiller, C. L., Stickler, A., Williams, J., and Lelieveld, J.: Hydroxyl radicals in the
19 tropical troposphere over the Suriname rainforest: airborne measurements, *Atmospheric Chemistry and Physics*, 10,
20 3759-3773, 2010.
- 21 Michoud, V., Colomb, A., Borbon, A., Miet, K., Beekmann, M., Camredon, M., Aumont, B., Perrier, S., Zapf, P.,
22 Siour, G., Ait-Helal, W., Afif, C., Kukui, A., Furger, M., Dupont, J. C., Haeffelin, M., and Doussin, J. F.: Study of
23 the unknown HONO daytime source at a European suburban site during the MEGAPOLI summer and winter field
24 campaigns, *Atmospheric Chemistry and Physics*, 14, 2805-2822, 2014.
- 25 Monge, M. E., D'Anna, B., Mazri, L., Giroir-Fendler, A., Ammann, M., Donaldson, D. J., and George, C.: Light
26 changes the atmospheric reactivity of soot, *Proceedings of the National Academy of Sciences of the United States of*
27 *America*, 107, 6605-6609, 2010.
- 28 Murphy, D. M., and Koop, T.: Review of the vapour pressures of ice and supercooled water for atmospheric
29 applications, *Quarterly Journal of the Royal Meteorological Society*, 131, 1539-1565, 10.1256/qj.04.94, 2005.
- 30 Nägele, W., and Conrad, R.: Influence of soil pH on the nitrate-reducing microbial populations and their potential to
31 reduce nitrate to NO and N₂O, *FEMS Microbiology Letters*, 74, 49-57, 1990.
- 32 Ndour, M., D'Anna, B., George, C., Ka, O., Balkanski, Y., Kleffmann, J., Stemmler, K., and Ammann, M.:
33 Photoenhanced uptake of NO₂ on mineral dust: Laboratory experiments and model simulations, *Geophysical*
34 *Research Letters*, 35, 2008.



- 1 Oswald, R., Behrendt, T., Ermel, M., Wu, D., Su, H., Cheng, Y., Breuninger, C., Moravek, A., Mougín, E., Delon,
2 C., Loubet, B., Pommerening-Roeser, A., Soergel, M., Poeschl, U., Hoffmann, T., Andreae, M. O., Meixner, F. X.,
3 and Trebs, I.: HONO Emissions from Soil Bacteria as a Major Source of Atmospheric Reactive Nitrogen, *Science*,
4 341, 1233-1235, 2013.
- 5 Oswald, R., Ermel, M., Hens, K., Novelli, A., Ouwersloot, H. G., Paasonen, P., Petaja, T., Sipila, M., Keronen, P.,
6 Back, J., Konigstedt, R., Beygi, Z. H., Fischer, H., Bohn, B., Kubistin, D., Harder, H., Martinez, M., Williams, J.,
7 Hoffmann, T., Trebs, I., and Soergel, M.: A comparison of HONO budgets for two measurement heights at a field
8 station within the boreal forest in Finland, *Atmospheric Chemistry and Physics*, 15, 799-813, 2015.
- 9 Paulson, S. E., Chung, M. Y., and Hasson, A. S.: OH radical formation from the gas-phase reaction of ozone with
10 terminal alkenes and the relationship between structure and mechanism, *Journal of Physical Chemistry A*, 103, 8125-
11 8138, 1999.
- 12 Pikridas, M., Bougiatioti, A., Hildebrandt, L., Engelhart, G. J., Kostenidou, E., Mohr, C., Prévôt, A. S. H.,
13 Kouvarakis, G., Zarmas, P., Burkhardt, J. F., Lee, B. H., Psichoudaki, M., Mihalopoulos, N., Pilinis, C., Stohl, A.,
14 Baltensperger, U., Kulmala, M., and Pandis, S. N.: The Finokalia Aerosol Measurement Experiment – 2008 (FAME-
15 08): an overview, *Atmos. Chem. Phys.*, 10, 6793-6806, 2010.
- 16 Pitts, J. N., Sanhueza, E., Atkinson, R., Carter, W. P. L., Winer, A. M., Harris, G. W., and Plum, C. N.: An
17 investigation of the dark formation of nitrous acid in environmental chambers, *International Journal of Chemical*
18 *Kinetics*, 16, 919-939, 1984.
- 19 Quastel, J. H.: Soil Metabolism, *Annual Review of Plant Physiology*, 16, 217-240, 1965.
- 20 Ramazan, K. A., Syomin, D., and Finlayson-Pitts, B. J.: The photochemical production of HONO during the
21 heterogeneous hydrolysis of NO₂, *Physical Chemistry Chemical Physics*, 6, 3836-3843, 2004.
- 22 Ren, X. R., Harder, H., Martinez, M., Leshner, R. L., Oligier, A., Simpas, J. B., Brune, W. H., Schwab, J. J.,
23 Demerjian, K. L., He, Y., Zhou, X. L., and Gao, H. G.: OH and HO₂ chemistry in the urban atmosphere of New
24 York City, *Atmospheric Environment*, 37, 3639-3651, 2003.
- 25 Ren, X., Brune, W. H., Oligier, A., Metcalf, A. R., Simpas, J. B., Shirley, T., Schwab, J. J., Bai, C., Roychowdhury,
26 U., Li, Y., Cai, C., Demerjian, K. L., He, Y., Zhou, X., Gao, H., and Hou, J.: OH, HO₂, and OH reactivity during the
27 PMTACS-NY Whiteface Mountain 2002 campaign: Observations and model comparison, *Journal of Geophysical*
28 *Research-Atmospheres*, 111, 2006.
- 29 Ren, X., Gao, H., Zhou, X., Crouse, J. D., Wennberg, P. O., Browne, E. C., LaFranchi, B. W., Cohen, R. C.,
30 McKay, M., Goldstein, A. H., and Mao, J.: Measurement of atmospheric nitrous acid at Blodgett Forest during
31 BEARPEX2007, *Atmospheric Chemistry and Physics*, 10, 6283-6294, 2010.
- 32 Ren, X., Sanders, J. E., Rajendran, A., Weber, R. J., Goldstein, A. H., Pusede, S. E., Browne, E. C., Min, K. E., and
33 Cohen, R. C.: A relaxed eddy accumulation system for measuring vertical fluxes of nitrous acid, *Atmospheric*
34 *Measurement Techniques*, 4, 2093-2103, 2011.



- 1 Rubio, M. A., Lissi, E., and Villena, G.: Nitrite in rain and dew in Santiago city, Chile. Its possible impact on the
2 early morning start of the photochemical smog, *Atmospheric Environment*, 36, 293-297, 2002.
- 3 Sander, S. P., J. Abbatt, J. R. Barker, J. B. Burkholder, R. R. Friedl, D. M. Golden, R. E. Huie, C. E. Kolb, M. J.
4 Kurylo, G. K. Moortgat, V. L. Orkin. and P. H. Wine: Chemical Kinetics and Photochemical Data for Use in
5 Atmospheric Studies, Evaluation No. 17, JPL Publication 10-6, Jet Propulsion Laboratory, Pasadena, 2011,
6 <http://jpldataeval.jpl.nasa.gov>.
- 7 Scharko, N. K., Berke, A. E., and Raff, J. D.: Release of Nitrous Acid and Nitrogen Dioxide from Nitrate Photolysis
8 in Acidic Aqueous Solutions, *Environmental Science & Technology*, 48, 11991-12001, 2014.
- 9 Soergel, M., Regelin, E., Bozem, H., Diesch, J. M., Drewnick, F., Fischer, H., Harder, H., Held, A., Hosaynali-
10 Beygi, Z., Martinez, M., and Zetzsch, C.: Quantification of the unknown HONO daytime source and its relation to
11 NO₂, *Atmospheric Chemistry and Physics*, 11, 10433-10447, 2011a.
- 12 Soergel, M., Trebs, I., Serafimovich, A., Moravek, A., Held, A., and Zetzsch, C.: Simultaneous HONO
13 measurements in and above a forest canopy: influence of turbulent exchange on mixing ratio differences,
14 *Atmospheric Chemistry and Physics*, 11, 841-855, 2011b.
- 15 Spataro, F., Ianniello, A., Esposito, G., Allegrini, I., Zhu, T., and Hu, M.: Occurrence of atmospheric nitrous acid in
16 the urban area of Beijing (China), *The Science of the total environment*, 447, 210-224, 2013.
- 17 Stemmler, K., Ammann, M., Donders, C., Kleffmann, J., and George, C.: Photosensitized reduction of nitrogen
18 dioxide on humic acid as a source of nitrous acid, *Nature*, 440, 195-198, 2006.
- 19 Stemmler, K., Ndour, M., Elshorbany, Y., Kleffmann, J., D'Anna, B., George, C., Bohn, B., and Ammann, M.: Light
20 induced conversion of nitrogen dioxide into nitrous acid on submicron humic acid aerosol, *Atmospheric Chemistry
21 and Physics*, 7, 4237-4248, 2007.
- 22 Stutz, J., Alicke, B., and Neftel, A.: Nitrous acid formation in the urban atmosphere: Gradient measurements of NO₂
23 and HONO over grass in Milan, Italy, *Journal of Geophysical Research-Atmospheres*, 107, 2002.
- 24 Su, H., Cheng, Y. F., Shao, M., Gao, D. F., Yu, Z. Y., Zeng, L. M., Slanina, J., Zhang, Y. H., and Wiedensohler, A.:
25 Nitrous acid (HONO) and its daytime sources at a rural site during the 2004 PRIDE-PRD experiment in China,
26 *Journal of Geophysical Research-Atmospheres*, 113, 2008a.
- 27 Su, H., Cheng, Y. F., Cheng, P., Zhang, Y. H., Dong, S., Zeng, L. M., Wang, X., Slanina, J., Shao, M., and
28 Wiedensohler, A.: Observation of nighttime nitrous acid (HONO) formation at a non-urban site during PRIDE-
29 PRD2004 in China, *Atmospheric Environment*, 42, 6219-6232, 2008b.
- 30 Su, H., Cheng, Y., Oswald, R., Behrendt, T., Trebs, I., Meixner, F. X., Andreae, M. O., Cheng, P., Zhang, Y., and
31 Poeschl, U.: Soil Nitrite as a Source of Atmospheric HONO and OH Radicals, *Science*, 333, 1616-1618, 2011.
- 32 Tang, Y., An, J., Wang, F., Li, Y., Qu, Y., Chen, Y., and Lin, J.: Impacts of an unknown daytime HONO source on
33 the mixing ratio and budget of HONO, and hydroxyl, hydroperoxyl, and organic peroxy radicals, in the coastal
34 regions of China, *Atmospheric Chemistry and Physics*, 15, 9381-9398, 2015.



- 1 VandenBoer, T. C., Brown, S. S., Murphy, J. G., Keene, W. C., Young, C. J., Pszenny, A. A. P., Kim, S., Warneke,
2 C., de Gouw, J. A., Maben, J. R., Wagner, N. L., Riedel, T. P., Thornton, J. A., Wolfe, D. E., Dubé, W. P., Öztürk,
3 F., Brock, C. A., Grossberg, N., Lefer, B., Lerner, B., Middlebrook, A. M., and Roberts, J. M.: Understanding the
4 role of the ground surface in HONO vertical structure: High resolution vertical profiles during NACHTT-11, *Journal*
5 *of Geophysical Research: Atmospheres*, 118, 10,155-110,171, 2013.
- 6 VandenBoer, T. C., Markovic, M. Z., Sanders, J. E., Ren, X., Pusede, S. E., Browne, E. C., Cohen, R. C., Zhang, L.,
7 Thomas, J., Brune, W. H., and Murphy, J. G.: Evidence for a nitrous acid (HONO) reservoir at the ground surface in
8 Bakersfield, CA, during CalNex 2010, *Journal of Geophysical Research-Atmospheres*, 119, 9093-9106, 2014.
- 9 VandenBoer, T. C., Young, C. J., Talukdar, R. K., Markovic, M. Z., Brown, S. S., Roberts, J. M., and Murphy, J. G.:
10 Nocturnal loss and daytime source of nitrous acid through reactive uptake and displacement, *Nature Geosci*, 8, 55-
11 60, 2015.
- 12 Villena, G., Kleffmann, J., Kurtenbach, R., Wiesen, P., Lissi, E., Rubio, M. A., Croxatto, G., and Rappenglueck, B.:
13 Vertical gradients of HONO, NO_x and O₃ in Santiago de Chile, *Atmospheric Environment*, 45, 3867-3873, 2011.
- 14 Vogel, B., Vogel, H., Kleffmann, J., and Kurtenbach, R.: Measured and simulated vertical profiles of nitrous acid -
15 Part II. Model simulations and indications for a photolytic source, *Atmospheric Environment*, 37, 2957-2966, 2003.
- 16 Wang, S. H., Ackermann, R., Spicer, C. W., Fast, J. D., Schmeling, M., and Stutz, J.: Atmospheric observations of
17 enhanced NO₂-HONO conversion on mineral dust particles, *Geophysical Research Letters*, 30, 2003.
- 18 Wang, L., Wang, W., and Ge, M.: Heterogeneous uptake of NO₂ on soils under variable temperature and relative
19 humidity conditions, *Journal of Environmental Sciences*, 24, 1759-1766, 2012.
- 20 Weber, B., Wu, D., Tamm, A., Ruckteschler, N., Rodriguez-Caballero, E., Steinkamp, J., Meusel, H., Elbert, W.,
21 Behrendt, T., Soergel, M., Cheng, Y., Crutzen, P. J., Su, H., and Poeschi, U.: Biological soil crusts accelerate the
22 nitrogen cycle through large NO and HONO emissions in drylands, *Proceedings of the National Academy of*
23 *Sciences of the United States of America*, 112, 15384-15389, 2015.
- 24 Wentzell, J. J. B., Schiller, C. L., and Harris, G. W.: Measurements of HONO during BAQS-Met, *Atmospheric*
25 *Chemistry and Physics*, 10, 12285-12293, 2010.
- 26 Wong, K. W., Tsai, C., Lefer, B., Haman, C., Grossberg, N., Brune, W. H., Ren, X., Luke, W., and Stutz, J.: Daytime
27 HONO vertical gradients during SHARP 2009 in Houston, TX, *Atmospheric Chemistry and Physics*, 12, 635-652,
28 2012.
- 29 Wong, K. W., Tsai, C., Lefer, B., Grossberg, N., and Stutz, J.: Modeling of daytime HONO vertical gradients during
30 SHARP 2009, *Atmospheric Chemistry and Physics*, 13, 3587-3601, 2013.
- 31 Yabushita, A., Enami, S., Sakamoto, Y., Kawasaki, M., Hoffmann, M. R., and Colussi, A. J.: Anion-Catalyzed
32 Dissolution of NO₂ on Aqueous Microdroplets, *The Journal of Physical Chemistry A*, 113, 4844-4848, 2009.



- 1 Yang, Q., Su, H., Li, X., Cheng, Y., Lu, K., Cheng, P., Gu, J., Guo, S., Hu, M., Zeng, L., Zhu, T., and Zhang, Y.:
- 2 Daytime HONO formation in the suburban area of the megacity Beijing, China, *Science China Chemistry*, 57, 1032-
- 3 1042, 2014.
- 4 Ye, C., Zhou, X., Pu, D., Stutz, J., Festa, J., Spolaor, M., Tsai, C., Cantrell, C., Mauldin, R. L., Campos, T.,
- 5 Weinheimer, A., Hornbrook, R. S., Apel, E. C., Guenther, A., Kaser, L., Yuan, B., Karl, T., Haggerty, J., Hall, S.,
- 6 Ullmann, K., Smith, J. N., Ortega, J., and Knote, C.: Rapid cycling of reactive nitrogen in the marine boundary layer,
- 7 *Nature*, 532, 489-491, 2016.
- 8 Zhou, X. L., Beine, H. J., Honrath, R. E., Fuentes, J. D., Simpson, W., Shepson, P. B., and Bottenheim, J. W.:
- 9 Snowpack photochemical production of HONO: a major source of OH in the Arctic boundary layer in springtime,
- 10 *Geophysical Research Letters*, 28, 4087-4090, 2001.
- 11 Zhou, X. L., Civerolo, K., Dai, H. P., Huang, G., Schwab, J., and Demerjian, K.: Summertime nitrous acid chemistry
- 12 in the atmospheric boundary layer at a rural site in New York State, *Journal of Geophysical Research-Atmospheres*,
- 13 107, 2002a.
- 14 Zhou, X. L., He, Y., Huang, G., Thornberry, T. D., Carroll, M. A., and Bertman, S. B.: Photochemical production of
- 15 nitrous acid on glass sample manifold surface, *Geophysical Research Letters*, 29, 2002b.
- 16 Zhou, X. L., Gao, H. L., He, Y., Huang, G., Bertman, S. B., Civerolo, K., and Schwab, J.: Nitric acid photolysis on
- 17 surfaces in low-NO_x environments: Significant atmospheric implications, *Geophysical Research Letters*, 30, 2003.
- 18 Zhou, X., Huang, G., Civerolo, K., Roychowdhury, U., and Demerjian, K. L.: Summertime observations of HONO,
- 19 HCHO, and O₃ at the summit of Whiteface Mountain, New York, *Journal of Geophysical Research-Atmospheres*,
- 20 112, 2007.
- 21 Zhou, X., Zhang, N., TerAvest, M., Tang, D., Hou, J., Bertman, S., Alaghmand, M., Shepson, P. B., Carroll, M. A.,
- 22 Griffith, S., Dusanter, S., and Stevens, P. S.: Nitric acid photolysis on forest canopy surface as a source for
- 23 tropospheric nitrous acid, *Nature Geoscience*, 4, 440-443, 2011.
- 24 Zhou, Y., Rosen, E. P., Zhang, H., Rattanavaraha, W., Wang, W., and Kamens, R. M.: SO₂ oxidation and nucleation
- 25 studies at near-atmospheric conditions in outdoor smog chamber, *Environmental Chemistry*, 10, 210-220, 2013.
- 26
- 27
- 28
- 29
- 30
- 31
- 32
- 33
- 34



1 **Table 1: Linear correlation factors (Pearson correlation, R^2) of HONO and the unknown source S_{HONO} to meteorological**
 2 **factors and different NO_x parameters.**

| | during the whole campaign | | | | |
|-------------------------------------|---------------------------|-------------------|--------------------------|--------------------------|---|
| | | | Time of day average | | |
| | HONO | S_{HONO} | HONO | S_{HONO} | |
| T | 0.006 | 0.135 | 0.488 | 0.227 | a highly correlated $R^2 > 0.8$ b moderate correlated $R^2 > 0.65$ c poorly correlated $R^2 > 0.5$ * anti-correlated |
| RH | 0.077 | 0.004* | 0.092 | 0.153 | |
| Heat flux | 0.261 | 0.300 | <i>0.617^c</i> | <i>0.648^c</i> | |
| J_{NO_2} | 0.263 | 0.414 | 0.718^b | 0.735^b | |
| NO | 0.242 | 0.206 | 0.857^a | <i>0.640^c</i> | |
| NO_2 | 0.052 | 0.091 | <i>0.620^c</i> | 0.438 | |
| NO_2 *RH | 0.126 | 0.135 | <i>0.638^c</i> | 0.457 | |
| NO_2 *RH*aerosol surface | 0.095 | 0.110 | 0.256 | <i>0.561^c</i> | |
| NO_2 *J | 0.191 | 0.189 | 0.828^a | 0.839^a | |
| NO_2 *RH*J | 0.266 | 0.258 | 0.850^a | 0.840^a | |
| NO_2 *RH*J*aerosol surface | 0.221 | 0.218 | 0.806^a | 0.848^a | |
| S_{NO} | | 0.010 | | 0.268 | |

| | during the humid period | | | | during the dry period | | | |
|-------------------------------------|-------------------------|-------------------|---------------------|--------------------------|--------------------------|-------------------|--------------------------|--------------------------|
| | | | Time of day average | | | | Time of day average | |
| | HONO | S_{HONO} | HONO | S_{HONO} | HONO | S_{HONO} | HONO | S_{HONO} |
| T | 0.006 | 0.126 | 0.031 | 0.113 | 0.120 | 0.013 | 0.453 | -0.015 |
| RH | 0.000 | 0.092* | 0.010* | 0.127* | 0.374 | 0.227 | 0.730^b | 0.683^b |
| Heat flux | 0.110 | 0.274 | 0.184 | <i>0.554^c</i> | <i>0.502^c</i> | 0.303 | 0.685^b | <i>0.594^c</i> |
| J_{NO_2} | 0.150 | 0.467 | 0.245 | 0.698^b | 0.678^b | 0.357 | 0.829^a | 0.657^b |
| NO | 0.168 | 0.188 | 0.418 | 0.676^b | 0.487 | 0.323 | 0.730^b | 0.302 |
| NO_2 | 0.066 | 0.075 | 0.300 | 0.353 | 0.037 | -0.002* | <i>0.619^c</i> | 0.171 |
| NO_2 *RH | 0.084 | 0.053 | 0.294 | 0.245 | 0.161 | 0.021 | 0.714^b | <i>0.523^c</i> |
| NO_2 *RH*aerosol surface | 0.047 | 0.079 | 0.111 | 0.147 | 0.241 | 0.106 | <i>0.557^c</i> | <i>0.621^c</i> |
| NO_2 *J | 0.214 | 0.291 | 0.427 | 0.910^a | 0.358 | 0.018 | 0.872^a | 0.657^b |
| NO_2 *RH*J | 0.231 | 0.271 | 0.467 | 0.850^a | 0.434 | 0.085 | 0.820^a | 0.770^b |
| NO_2 *RH*J*aerosol surface | 0.140 | 0.160 | 0.465 | 0.784^b | 0.414 | 0.171 | 0.664 ^b | 0.678^b |
| S_{NO} | | 0.323 | | 0.778^b | | 0.003* | | -0.009* |



Figure 1: Map of location: the red star shows the location of Ineia and the measuring site. The four red points mark the main cities of Cyprus, Nicosia, Larnaca, Limassol and Paphos (clockwise ordering), map produced by the Cartographic Research Lab University of Alabama, map of Cyprus: google maps.

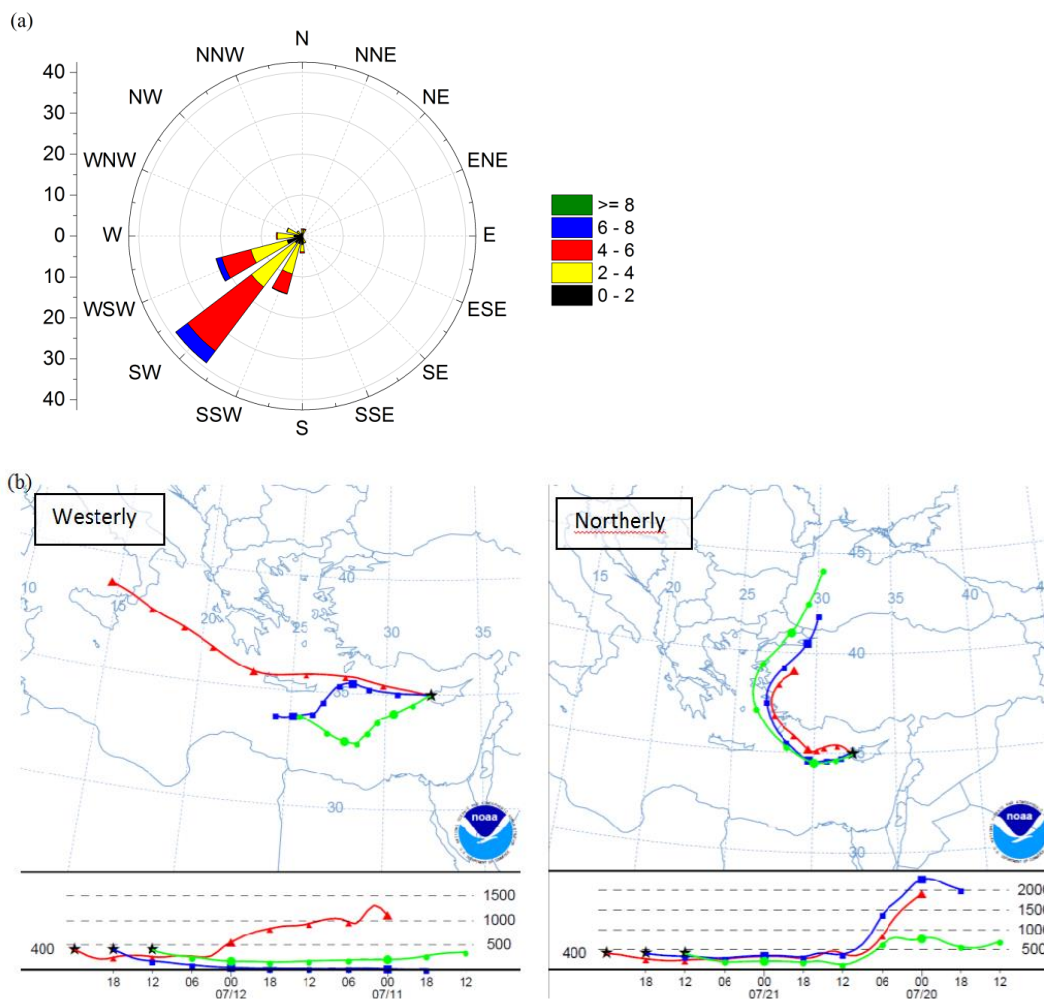


Figure 2: Airflow conditions during the CYPHEX campaign: a) Measured local wind direction, b) back trajectories calculated with NOAA Hysplit model showing examples for the two main air mass origins (48 hours, UTC = LT - 3 h).

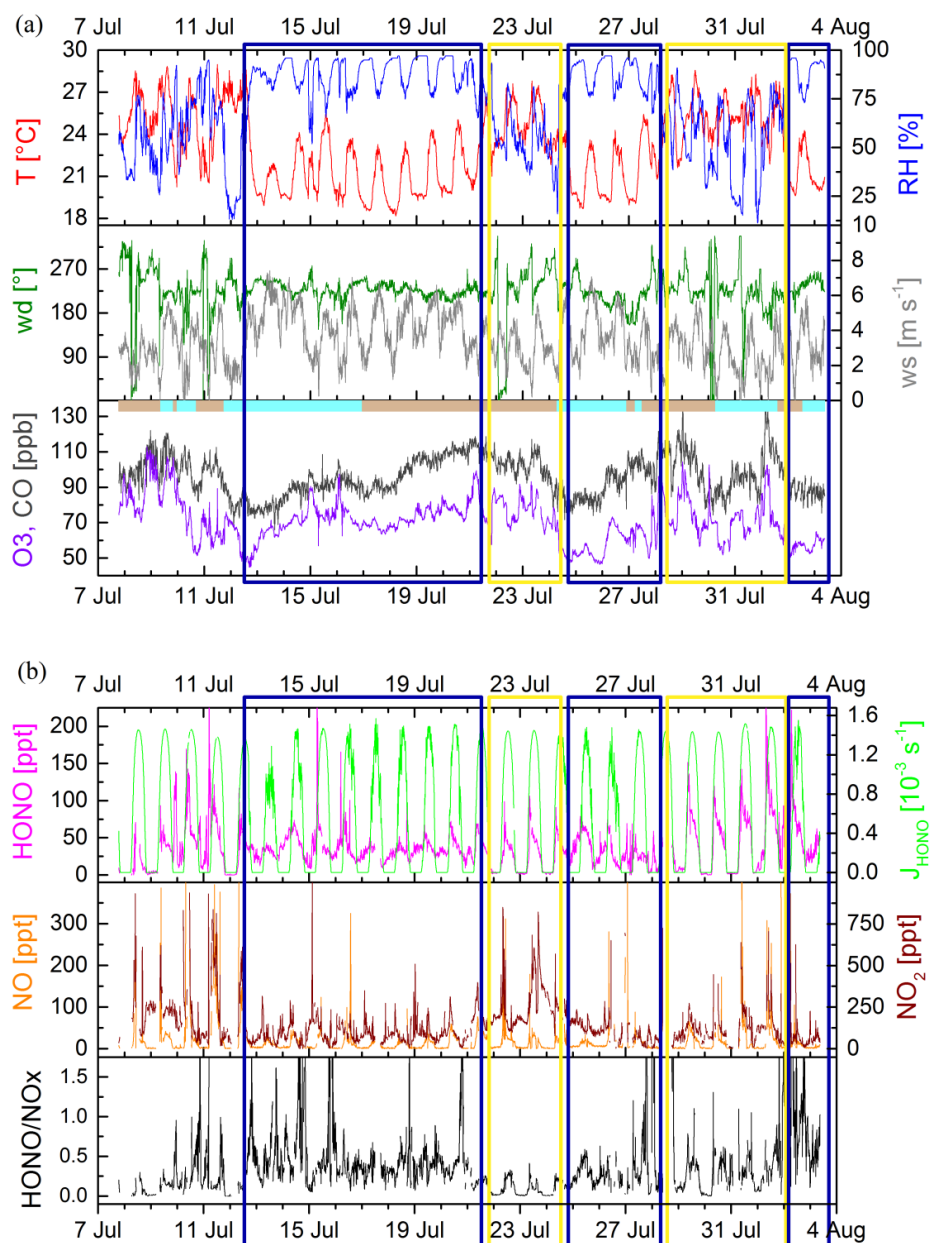


Figure 3: Measured variables during the whole campaign from 7th July to 4th August 2014, a) meteorological data (Temperature T, relative humidity RH, wind direction and speed wd, ws) and O₃ and CO indicating stable conditions, in the lower panel the bar indicates the air mass origin: bright blue = westerly, brownish = northerly, b) observed mixing ratios of HONO, NO₂ and NO, and the photolysis frequency J_{HONO} and the HONO/NO_x ratio. The yellow and blue boxes reflect the dry and the humid periods, respectively.

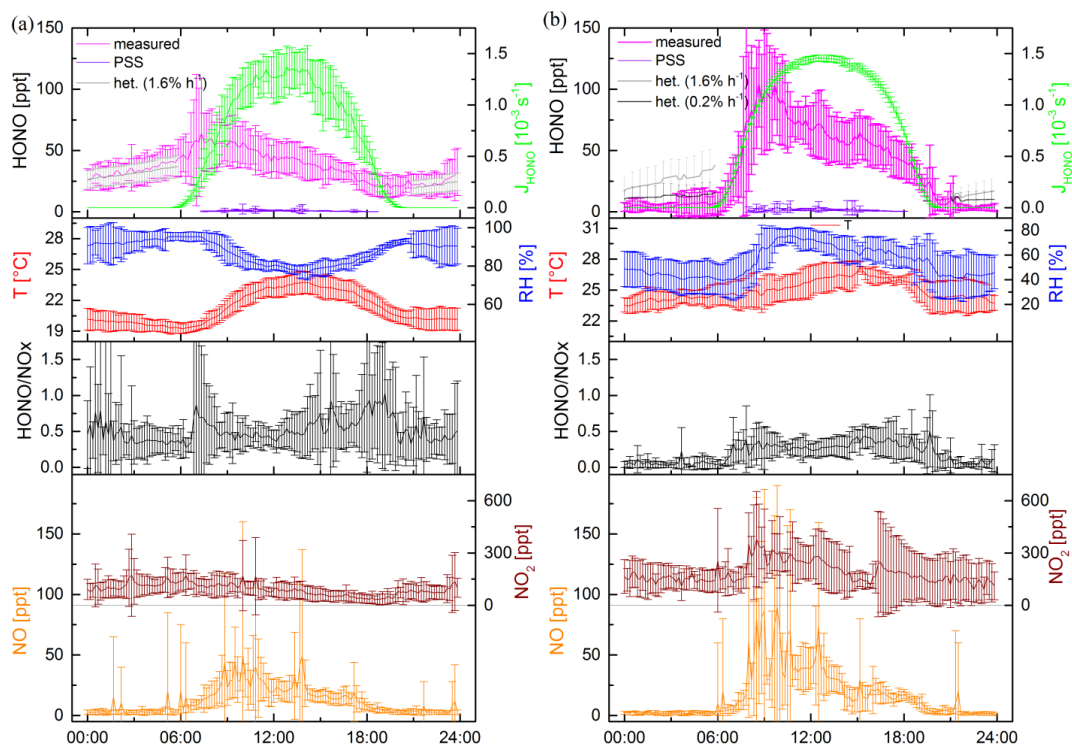


Figure 4: Diel variation of meteorological data (Temperature T , relative humidity RH), NO and NO_2 mixing ratios, the photolysis rate for HONO J_{HONO} and HONO mixing ratios (pink: measured, violet: daytime photostationary state PSS, grey: nighttime heterogeneous NO_2 conversion) and HONO/ NO_x ratio for a) average for period when RH was above 60% (blue box in Fig. 3) and b) average for dry period when RH was below 60% (yellow box in Fig. 3).

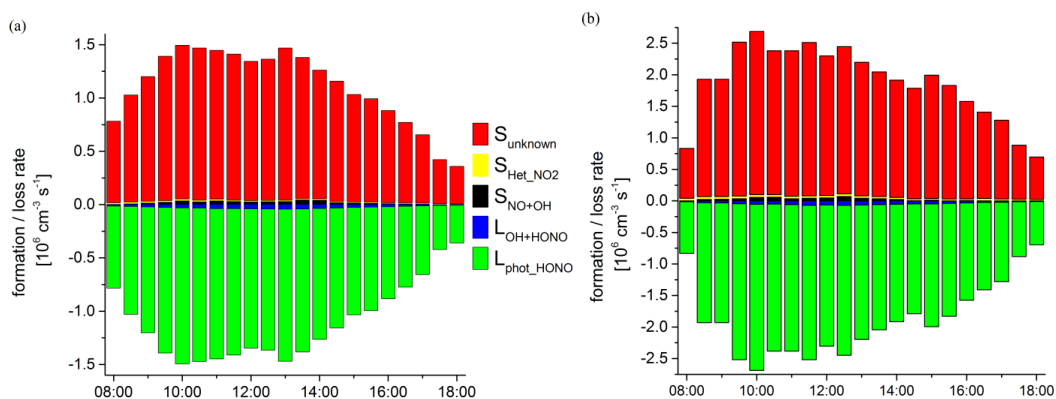


Figure 5: HONO budget analysis for a) the humid and b) the dry period. S_{OH+NO} (black) stands for the formation rate of HONO via the reaction of NO and OH , $S_{Het_NO_2}$ (yellow) is the formation rate for the heterogeneous reaction of NO_2 (conversion rate $1.6\% h^{-1}$), L_{phot} (green) and $L_{OH+HONO}$ (blue) are the loss rates via photolysis and the reaction with OH and $S_{unknown}$ is the unknown source.

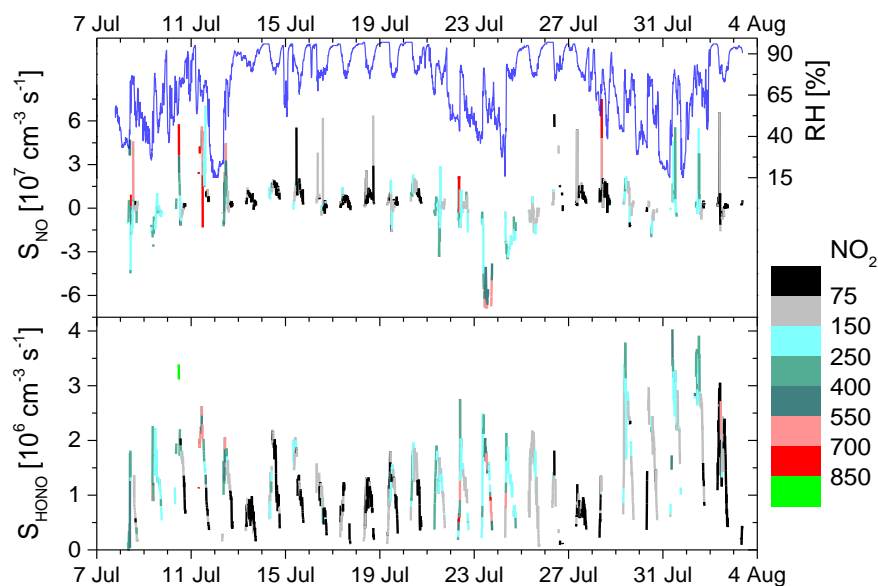


Figure 6: NO_2 (color-coded) and RH dependence of the sources of NO (S_{NO}) and HONO (S_{HONO}).

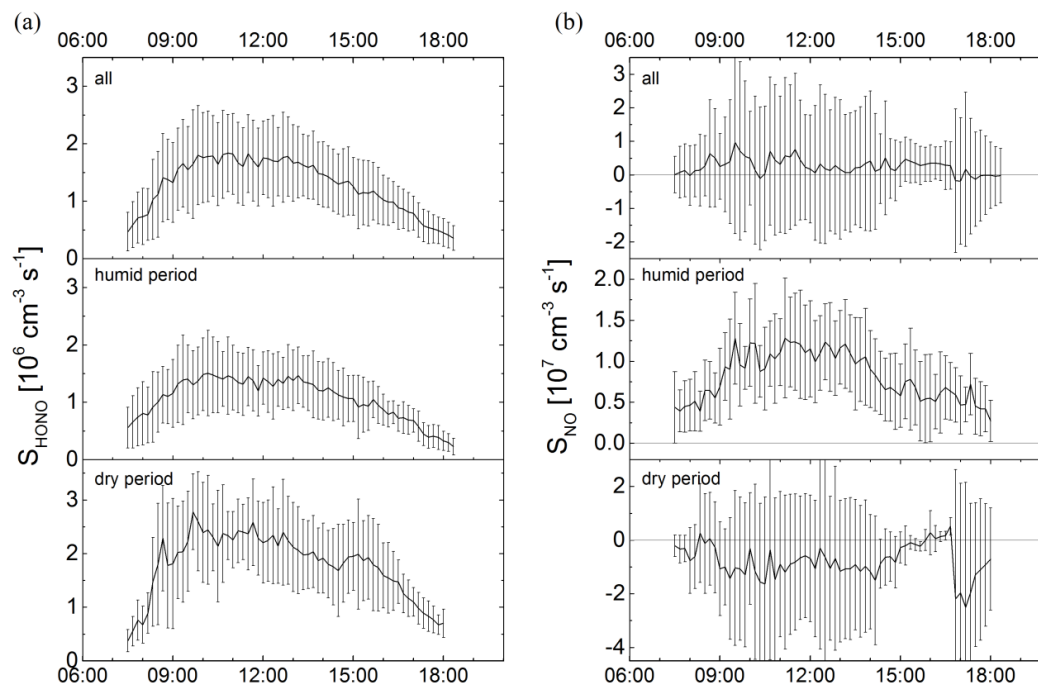


Figure 7: Diel profile of both unknown sources S_{HONO} (a) and S_{NO} (b) for all data, humid (excluding transition days: 25.7. and 2.8 and 15.7. as RH conditions changed too quickly) and dry periods.

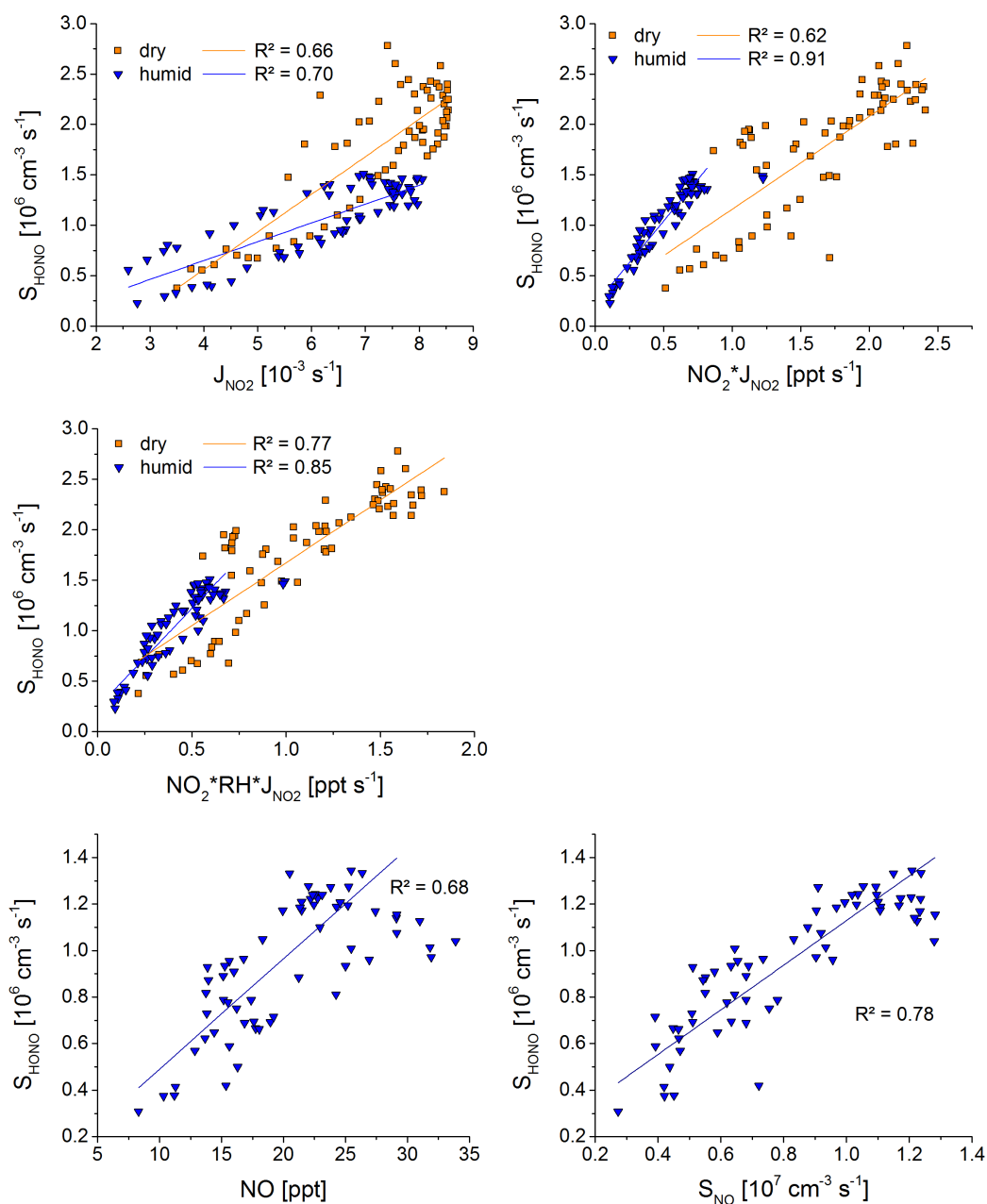


Figure 8: Correlation of S_{HONO} to light induced NO_2 reaction (for both periods, humid = blue triangle, dry = orange square), to NO and S_{NO} (only for humid period); time of day average data were used (S_{HONO} and NO; S_{HONO} and S_{NO} excluding the 3 days mentioned before).

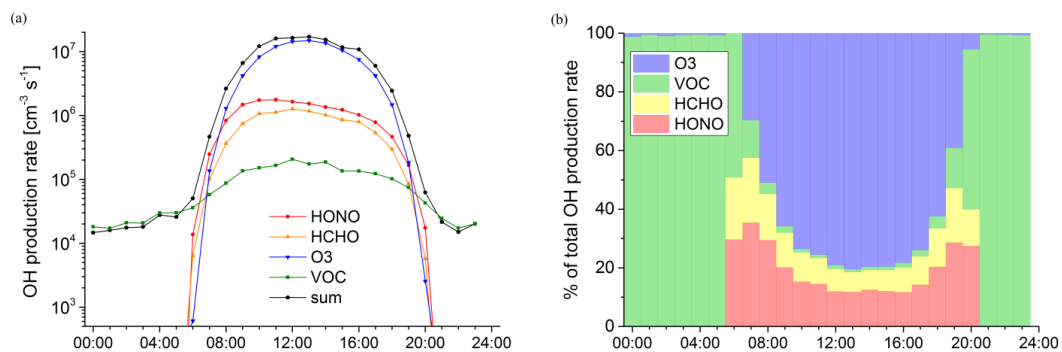


Figure 9: Average diel pattern of OH production from HONO, O₃, HCHO and VOC, a) shown as production rate and b) percentage contributions to total OH production.